UNIVERSIDADE FEDERAL DO CEARÁ
CENTRO DE TECNOLOGIA
DEPARTAMENTO DE ENGENHARIA QUÍMICA
PROGRAMA DE PÓS-GRADUAÇÃO EM ENGENHARIA QUÍMICA

KLAUS FEIO SOARES RICHARD

EVALUATION OF INTRAPARTICLE MASS TRANSFER PROPERTIES BY MICROCALORIMETRY

FORTALEZA

2020

KLAUS FEIO SOARES RICHARD

EVALUATION OF INTRAPARTICLE MASS TRANSFER PROPERTIES BY MICROCALORIMETRY

Dissertação apresentada ao Curso de Engenharia Química da Universidade Federal Do Ceará, como requisito parcial para obtenção do título de mestre em Engenharia Química. Área de concentração: Processos Químicos e Bioquímicos.

Orientador: Prof. Dr. Moisés Bastos Neto
Coorientadora: Profa. Dra. Diana Cristina Silva de Azevedo

FORTALEZA

2020

Dados Internacionais de Catalogação na Publicação
Universidade Federal do Ceará
Biblioteca Universitária
Gerada automaticamente pelo módulo Catalog, mediante os dados fornecidos pelo(a) autor(a)

R385e Richard, Klaus Feio Soares.
Evaluation of intraparticle mass transfer properties by microcalorimetry / Klaus Feio Soares Richard. – 2020.
93 f. : il. color.

Dissertação (mestrado) – Universidade Federal do Ceará, Centro de Tecnologia, Programa de Pós-Graduação em Engenharia Química, Fortaleza, 2020.
Orientação: Prof. Dr. Moisés Bastos Neto.
Coorientação: Prof. Dr. Diana Cristina Silva de Azevedo.

1. Adsorção. 2. Difusão. 3. Microcalorimetria. 4. Modelagem. I. Título.

CDD 660

KLAUS FEIO SOARES RICHARD

EVALUATION OF INTRAPARTICLE MASS TRANSFER PROPERTIES BY MICROCALORIMETRY

Dissertation presented to the department of Chemical engineering of Universidade Federal do Ceará, as a partial requisite to obtain the Master's degree in Chemical Engineering. Concentration Area: Chemical and Biochemical Processes.

Approved at: 27/ 02 / 2020

DISSERTATION COMMITTEE

_____

Prof. Dr. Moisés Bastos Neto (Advisor)

Universidade Federal do Ceará (UFC)

_____

Prof. Dr. Diana Cristina Silva de Azevedo (Co-advisor)

Universidade Federal do Ceará (UFC)

_____

Prof. Dr. Samuel Jorge Marques Cartaxo

Universidade Federal do Ceará (UFC)

_____

Prof. Dr. Marcio Schwaab

Universidade Federal do Rio Grande do Sul (UFRGS)

For you:

Mother, Suzi Cristina.

Sister, Raíssa.

Love, Náyade.

Nephews, Laura e Johann.

Goddaughter, Maria Esther.

ACKNOWLEDGEMENTS

To Náyade Santos, my great love, for softening my thoughts that are usually too focused on the objectives and for the happiness and motivation given to my sometimes cold heart.

To my dear mother, Suzi Cristina, for the protection and wisdom given to me to deal with life.

To my sister, Raíssa, for reminding of not taking myself too seriously all the time.

To my family, for the ever present support.

To PETROBRAS, for the funding of my Graduation study.

To my advisors, Prof. Dr. Moisés Bastos Neto and Prof. Dr. Diana Cristina Silva de Azevedo, for introducing and guiding me through the academy.

To Prof. MSc. Antonio Eurico Belo Torres for being always present in the construction of my dissertation, solving the problems alongside me.

To Dra. Débora Aline Soares Maia and Undergraduate Wagner de Sousa for helping me with the experimental part of the dissertation, which i lacked experience.

To Prof. Dr. Célio Loureiro Cavalcante Jr. For helping me solving very diffuse problems on the literature.

To Prof. Antonio Souza de Araújo, from Instituto de Química UFRN,for synthesizing fundamental material required for the dissertation.

To my colleagues of LPACO_2 for all the cooperation.

“No thief, however skillful, can rob one of knowledge,
and that is why knowledge is the
best and safest treasure to acquire.”

- L. Frank Baum

RESUMO

Um novo método para a avaliação de coeficientes de transferência de massa intrapartículas em adsorventes porosos foi desenvolvido e testado. O uso de microcalorimetria para a estimativa de coeficientes de difusão é um conceito convincente, porque a técnica - já amplamente usada para medir propriedades de equilíbrio - também pode ser usada como uma alternativa para avaliar propriedades cinéticas em um único experimento. Um microcalorímetro Tian-Calvet acoplado a uma configuração manométrica / volumétrica foi usado para os experimentos. Um modelo de adsorção não isotérmica foi derivado para o sistema, com o fenômeno de transferência de massa sendo modelado de acordo com diferentes abordagens: uma é o modelo de Linear Driving Forece (LDF), proposto por Glueckauf (1955); E o outro é o modelo de controle difusional intrapartícula, desenvolvido para estimar a constante de tempo difusional, D_c/R^2. O modelo proposto foi analisado e testado quanto à sua sensibilidade paramétrica, permitindo a determinação dos limites de medição. Dados experimentais para uma ampla variedade de adsorventes foram simulados e os parâmetros correspondentes estimados. O método apresentado mostrou uma capacidade razoável para estimar as propriedades de transferência de massa, apesar de algumas restrições experimentais e limitações de sensibilidade para espécies de rápida difusão.

Palavras-Chave: Adsorção; Difusão; Microcalorimetria; Modelagem;

ABSTRACT

A novel method for the assessment of intraparticle mass transfer coefficients in porous adsorbents has been developed and tested. The use of microcalorimetry for the estimation of diffusion coefficients is a compelling concept because the technique – already widely used to measure equilibrium properties – might be also used as an alternative to evaluate kinetic properties in a single experiment. A Tian-Calvet microcalorimeter coupled with a manometric/volumetric setup has been used for the experiments. A non-isothermal adsorption model has been derived for the system, with the mass transfer phenomenon being modelled according to different approaches: one is the Linear Driving Force (LDF) model, proposed by Glueckauf (1955); and the other is the intraparticle diffusional control model, developed to estimate the diffusional time constant, D_c/R^2. The proposed model has been analyzed and tested for its parametric sensibility, allowing the determination of the measurement limits. Experimental data for a wide variety of sorbents were simulated and the corresponding parameters estimated. The presented method has shown a reasonable capability to estimate the mass transfer properties despite some experimental constraints and sensibility limitations for fast-diffusing species.

Keywords: Adsorption; Diffusion; Microcalorimetry; Modeling;

LIST OF FIGURES

LIST OF TABLES

LIST OF SYMBOLS

A_1	Lateral Dosing vessel área (m²)
A_2	Lateral Transfer Line área (m²)
A_3	Lateral Microcalorimetric cell wall área (m²)
A_{cw0}	Outer microcalorimetric cell wall área (m²)
α	Exponential pressure descrease parameter for adsorption model (1/s)
α_2	Exponential pressure descrease parameter for desorption model (1/s)
b	Affinity parameter, isotherm models (1/Pa)
β_n	Quadratic equation parameter of ZLC equation
C_1	Gas concentration at Dosing vessel (mol/m^3)
C_2	Gas concentration at transfer line (mol/m^3)
C_3	Gas concentration at microcalorimetric cell (mol/m^3)
C_{BET}	BET Concentration parameter (mol/m^3)
C_e	Equilibrium concentration (mol/m^3)
C_s	BET model saturation concetration (mol/m^3)
c_0	Initial fluid concentration, ZLC model (mol/m^3)
c_v	Molar heat capacity of gas (J/kg.K)
c_{ps}	Heat capacity of adsorbent (J/kg.K)
c_{pw}	Heat capacity of calorimeter wall (J/kg.K)
c	Fluid concentration (mol/m^3)
D	Overall diffusion coefficient (m²/s)
D_∞	Micropore diffusion coefficient at infinite temperature. (m²/s)
D_{AB}	Molecular diffusion coefficient (m²/s)
D_K	Knudsen diffusion coefficient (m²/s)
D_L	Axial dispersion (m²/s)
D_a	Sorbate diffusivity (m²/s)
D_{a0}	Thermodynamic Sorbate diffusivity (m²/s)
D_c	Intracrystaline diffusivity (m²/s)
D_{c0}	Intracrystaline Themodynamic diffusivity (m²/s)
D_{eff}	Effective diffusivity (m²/s)
D_p	Macropore diffusion coefficient (m²/s)
D_s	Diffusion coefficient due to surface diffusion (m²/s)

D_{vis}	Diffusion coefficient due to plug flow (m²/s)
E	Activaction Energy (J)
ϵ	Fixed bed porosity
ϵ_p	Particle porosity
f	Diffusivity temperature function
h_1	Heat transfer coefficient between gas and Dosing vessel wall (W/m²K)
h_2	Heat transfer coefficient between gas and Tranfer Line wall (W/m²K)
h_3	Heat transfer coefficient between gas and microcalorimeter cell wall (W/m²K)
$\widehat{H_{in}}$	Specific enthalpy of gas entering microcalorimetric cell wall (J/mol)
ΔH_{ads}	Enthalpy of Adsorption (J/mol)
J_a	Sorbate flux (mol/m².s)
k_{LDF}	Linear Driving force constant (1/s)
k_{cw}	Calorimeter wall thermal conductivity (W/m.K)
k_f	Film Mass transfer coefficient (1/s)
K	Calorimeter heat flow constant (W/K)
K_F	Freundlich equilibrium constant
K_H	Henry equilibrum constant
L	Spatial parameter at ZLC model
l	ZLC column length (m)
M	Molar mass of fluid (g/mol)
m_∞	Equilibrium adsorbed mass (kg)
m_s	Adsorbent mass at microcalorimeter (kg)
m_t	Adsorbed mass at a given time (kg)
m_{w1}	Tubing mass at dosing vessel (kg)
m_{w2}	Tubing mass at transfer line (kg)
μ	Chemical potential (J)
n_1^I	Number of moles of gas in Dosing vessel at equilibrium point number one (mol).
n_1^{II}	Number of moles of gas in Dosing vessel at equilibrium point number two (mol).
n_2^I	Number of moles of gas in Transfer Line at equilibrium point number one (mol).

n_2^{II}	Number of moles of gas in Transfer line at equilibrium point number two (mol).
n_3^{I}	Number of moles of gas in microcalorimeter at equilibrium point number one (mol).
n_3^{II}	Number of moles of gas in microcalorimeter at equilibrium point number two (mol).
n_{ads}^{I}	Number of moles of adsorbed gas at equilibrium point number one (mol).
n_{ads}^{II}	Number of moles of adsorbed gas at equilibrium point number two (mol).
n_{out}	Molar flowrate leaving dosing vessel (mol/s).
n_{outd}	Molar flowrate leaving microcalorimetric cell, desorption model (mol/s)
Δn_{ads}	Number of moles adsorbed between two equilibrum points (mol)
$\dot{n_{in}}$	Molar flowrate entering microcalorimetric cell (mol/s)
η	Fluid Viscosity (Pa.s)
P_1^I	Dosing Vessel pressure at equilibrium point number two (Pa)
P_1^{II}	Dosing vessel pressure at equilibrium point number two (Pa)
P_2^I	Transfer line pressure at equilibrum point number one (Pa).
P_2^{II}	Tranfer line pressure at equilibrium point number two (Pa).
P_3^I	Microcalorimetric cell pressure at equilibrum point number one (Pa).
P_3^{II}	Microcalorimetric cell pressure at equilibrium point number two (Pa).
P_E	Equilibrium Pressure at experimente (Pa)
p_a	Partial pressure of sorbate (Pa)
$\bar{q}$	Specific adsorbed concentration (mol/kg)
q_{BET}	BET model maximum adsorbed concentration parameter (mol/m^3)
q_E	Specific equilibrium adsorbed concentration (mol/kg)
q_e	Equilibrium adsorbed concentration (mol/m^3)
q_{avg}	Averaged bed adsorbed concentration (mol/m^3)
q_m	Maximum adsorbed concentration, isotherm models (mol/m^3)
$\dot{Q}$	Heat rate reported on the microcalorimetric experimente (W)
Q_{ads}	Heat transferred due to adsorption (J)
Q_{tot}	Total heat transferred in the microcalorimetry experiment (J)
q	Adsorbed concentration (mol/m^3)
r	Radial coordinate, diffusion models (m)
R_g	Gas constant (J/mol.K)

R_p	Particle radius (m)
r_a	Dimensionless radial coordinate, micropore diffusional model
r_c	Crystal radius of the sorbent (m)
r_{cw}	Radial coordinate for the conduction at calorimeter wall (m)
R_{cw}	Inner radius of microcalorimetric cell (m)
R_{cw0}	Outer radius of microcalorimetric cell (m)
ρ_{cw}	Cell wall density (kg/ m³)
ρ_p	Adsorbent density (kg/ m³)
T_1	Gas temperature at dosing vessel (K)
T_2	Gas temperature at transfer line (K)
T_3	Gas temperature at microcalorimetric cell (K)
T_{cw}	Calorimeter wall temperature (K)
T_{o1}	Ambient Temperature (K)
T_{o2}	Microcalorimeter controlled temperature (K
T	Generic Temperature (K)
t	Time (s)
U	Gas internal energy (J)
$\widehat{U_{in}}$	Specific Internal energy of the gas entering the microcalorimetric cell (J/mol)
u_a	Sorbate velocity (m/s)
V_1	Dosing Vessel volume (m³)
V_2	Tranfer Line volume (m³)
V_3	Microcalorimetric cell volume (m³)
$\dot{V}_3$	Volumetric molar flow (mol/s)
v	Fluid velocity (m/s)
y_s	Fraction of fluid molecules on the solid surface
y_p	Fraction of fluid molecules in the pore surface
z	Axial Coordinate, Chromatographic column model (m)

SUMMARY

1 INTRODUCTION

The estimation of mass transfer properties in the process of diffusion in porous solids is of interest in both the pure sciences fields and in engineering. These solids have a wide range of applicability as adsorbents and catalysts that are essential for many processes in the chemical process industry and have attracted more attention in the recent years in newer practical applications such as the delivery of medicines (Laeri *et al.*, 2003). Description of the diffusion phenomena is also necessary for the modelling of well-established processes such as fixed bed adsorption (Ruthven, 1984) and Pressure Swing Adsorption, PSA (Ruthven,1994).

In addition to the practical use of the study of diffusion in porous solids, new insights on the field also lead to better understanding of the interaction between solid surfaces and molecules (Ertl, 2008) and the behavior of molecular systems of reduced dimensionality (Drake and Klafter, 1990). Leading to better and more detailed models to extend even further the applicability's that already exist or to discover new ones.

There are many well-established methods for estimating diffusional properties, these are generally divided in "microscopic" and "macroscopic" as described in Kärger et al (2011), and in general, as described by the same authors, the "macroscopic" methods provide results that are more applicable for practical processes. The main challenge involving the determination of diffusion coefficients is the proper evaluation of the mass and heat transfer resistances. Incorrect assumptions may lead to considerable errors and disagreement between two different methods. The same challenge also makes it difficult to measure the coefficients of fast-diffusion species, such as CO_2 and CH_4 (Kärger *et al.*, 2011).

Microcalorimetry of adsorption is a well-developed field dedicated to study the thermal phenomena and properties of adsorption in porous media, the developed methods involve the calculations of important thermodynamic properties of adsorbent-adsorbate systems such as the Enthalpy of Adsorption, and energetic description of porous solids through the experiments. These parameters and description also contribute to the modeling of the previous mentioned mass-transfer models used in practical applications.

The objective of this work is to propose and analyze a novel "macroscopic" method for estimating intraparticle diffusion through microcalorimetry. The proposal involves correlating the mass transfer parameters with the heat rate measures of the microcalorimeter by applying proper models and the analysis involves evaluating the reliability and robustness in face of the existing challenges and the already existing methods.

2 REVIEW

2.1 General Adsorption Fundamentals

Adsorption is a physical or chemical phenomenon where a chemical species in a fluid concentrates itself on the surface of a solid, spontaneously, due to a chemical potential gradient. This process reduces the concentration of the compound in the fluid until a thermodynamic equilibrium is reached. The adsorbed species is the adsorbate and the solid is the adsorbent. Adsorbents have different affinities for different compounds, some are attracted to the surface more than others are, and this difference is the principle of the use of adsorption to separate different chemicals. Detailed theoretical description of the phenomenon can be found in Ruthven (1984) and Do (1998).

The amount of a compound, which is adsorbed by a solid, in equilibrium, can be correlated with bulk fluid concentration, for liquid adsorbates, and partial pressure, for gaseous adsorbates. These correlations are constructed in graphs known as adsorption or equilibrium isotherms. Different adsorbent-adsorbate systems will exhibit different forms of isotherms; the most recent report of IUPAC (Thommes *et al*., 2015) discusses these types of curves, which are shown in Figure 2.1.

Figure 2.1 – Types of adsorption isotherms

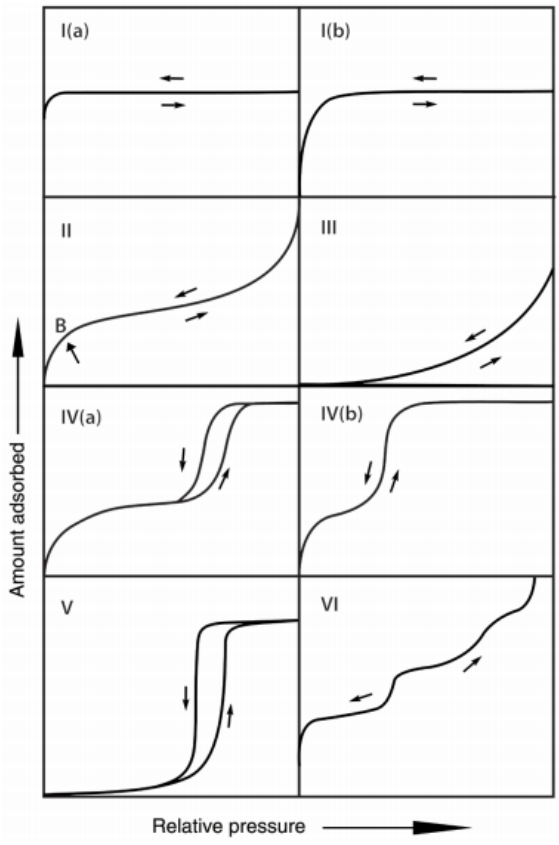

Source : Thommes *et al.* (2015)

2.1.1 Equilibrium Models

Equilibrium models for adsorption, also known as adsorption isotherms, are equations that are meant to appropriately correlate the adsorbed quantity of a species with a measurable property, such as concentration, in a fixed temperature. Some models are derived from theory, such as the Henry Law limit for low concentrations, and the Langmuir Isotherm, which assumes that the adsorption happens in a monolayer and that the solid is energetically homogeneous, most models, however, are semi-empirical.

Table 2.1 lists some models that were reviewed by Foo and Hameed (2010). In principle, it is possible to choose a model based on the adsorbate-adsorbent system properties, but generally, as discussed in Limousin *et al*. (2007), there is some trial and error. The choice escalates from trying to fit simpler models to more complex one by addition of parameters and modification of the equations to improve the model fit to the experimental data.

Table 2.1 – Some Adsorption Isotherm Models.

Isotherm	Equation	Application Example	Reference
Henry Law	$q_e = K_H C_e$	Low concentration sorption	Classical Thermodynamics
Langmuir	$q_e = \frac{q_m b C_e}{1 + b C_e}$	Methylene blue by Activated carbon	Langmuir (1916)
Freundlich	$q_e = K_F C_e^{\frac{1}{n}}$	Ammonium by Zeolites	Freundlich (1906)
Sips	$q_e = \frac{q_m b C_e^n}{1 + b C_e^n}$	CO_2 by activated carbon	Sips (1948)
Toth	$q_e = \frac{q_m b C_e}{(1 + b C_e^n)^{\frac{1}{n}}}$	H_2 by activated carbon	Toth (1971)
BET	$q_e = \frac{q_{BET} C_{BET} C_e}{(C_s - C_e)[1 + (C_{BET} - 1)\left(\frac{C_e}{C_s}\right)}$	Nitrogen at 77K in various sorbents	Brunauer et al (1938)

Source: Modified from Foo and Hameed (2010)

2.1.2 Kinetic models and diffusion mechanisms

The transport of chemical species through the adsorbent pores can by described by a diffusional process which has the driving force from the chemical potential as first recognized by Einstein (1906). The form of the energy balance of a differential element of diffusion is given by Equation 2.1

$$f u_a = -\frac{d\mu}{dz} \tag{2.1}$$

Applying the thermodynamic definition of chemical potential and applying the definition of flux, Equation 2.2 is derived.

$$J_a = u_a c = -\frac{R_g T}{f} \frac{d ln p_a}{d ln c} \frac{dc}{dz} \tag{2.2}$$

Diffusivity can be defined by the following terms of Equation 2.3

$$D_a = \frac{R_g T}{f} \frac{dlnp_a}{dlnc} \tag{2.3}$$

Which can be rearranged to express the thermodynamically corrected diffusivity as described by Darken(1948) , Equation 2.4.

$$D_a = D_{a0} \frac{dlnp_a}{dlnc_a} \tag{2.4}$$

The accurate description of the diffusion of species in porous adsorbents is dependent on the pore size relative to particle size of the system. IUPAC (Sing *et al.*, 1985) defines three main types of pores based on size; Macropores have widths exceeding about 50 nm; Mesopores comprise between 2 nm and 50 nm and Micropores have widths below 2nm.

For diffusion in macropores, four types of mechanisms can be identified; Molecular diffusion, for when the relative size of the molecules in comparison with the pores is small; Knudsen Diffusion, when the macropore is narrow in relation with the molecules size; Surface Diffusion, when there is significant adsorption at the pore walls and Plug flow. Considering a Fickian form of the diffusional flux, Equation 2.5 the diffusivities, in order of the citation of the mechanisms is shown in Equations 2.6 to 2.9.

$$J = -D \frac{dc}{dz} \tag{1.5}$$

$$D = D_{AB} \tag{2.6}$$

$$D = D_K = 97r \left(\frac{\sqrt{T}}{\sqrt{M}}\right) \tag{2.7}$$

$$D = D_p y_p + D_s y_s \tag{2.8}$$

$$D_{vis} = \frac{Pr^2}{8\eta} \tag{2.9}$$

For diffusion in micropores, diffusivity can be described as an exponential function of temperature, Equation 2.10 and the general equation for diffusion in micropores in a spherical particle is described by Equation 2.11.

$$D_c = D_\infty \, e^{-\frac{E}{R_g T}} \tag{2.10}$$

$$\frac{\partial q}{\partial t} = \frac{1}{r^2}\frac{\partial}{\partial r}\left(r^2 D_c \frac{\partial q}{\partial r}\right) \tag{2.11}$$

More detailed description of diffusion mechanisms and models are to be found in Kärger et al (2011), Do (1998), Nicholson and Petropoulos (1985) and Bathia *et al.* (2004).

2.2 Experimental Methods for diffusion Measurement

Macroscopic methods for intraparticle diffusivity measurements focuses on measuring the sorption rate in a system where the adsorbent is subjected to a well-defined change in concentration or pressure. The methods yield the diffusional time constant, $\frac{D}{R_p^2}$, which is the effective diffusivity per unit of the square radius of the particle or crystal. A brief description of the most used methods will be included.

2.2.1 Gravimetric Methods

These methods provide a straightforward measurement of diffusivities with the use of scales. The sorbate is subjected to step pressure changes, usually in a large system where total pressure is maintained constant, and the equipment tracks the response curve of $1 - \frac{m_t}{m_\infty}$ versus time, Figure 2.2. Careful evaluation of external heat transfer and mass transfer need to be taken into account before applying diffusional models, as the intraparticle mass transfer resistance needs to be significant for the measurement of diffusivities.

Figure 2.2 – Gravimetric sorption response curve

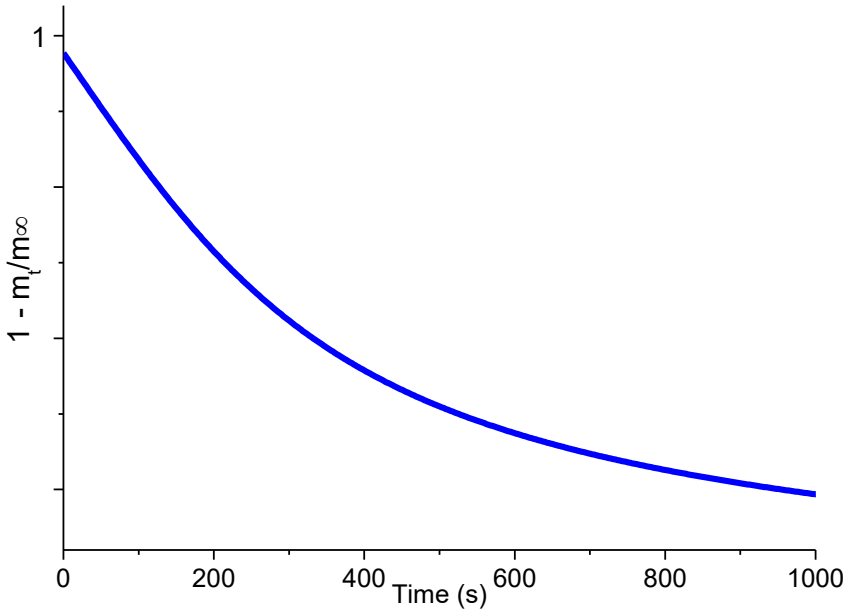

Source : Author

Equation 2.12 describes the response curve in a spherical particle for negligible external heat and mass transfer effects.

$$\frac{m_t}{m_\infty} = 1 - \frac{6}{\pi^2}\sum_{n=1}^{\infty}\frac{1}{n^2}e^{\left(\frac{n^2\pi^2 Dt}{R_p^2}\right)} \tag{2.12}$$

More detailed discussion on the method and addition of extra mass transfer resistances can be found in Keller and Staudt (2006) and Lee and Ruthven (1981).

2.2.2 Piezometric Methods

A piezometric method for measuring diffusion coefficients consists in tracking the pressure change in a system of constant volume containing an adsorbent sample, when this sample is subjected by a step pressure change of sorbate. Represented by Figure 2.3.

Figure 2.3 – Piezometric sorption system.

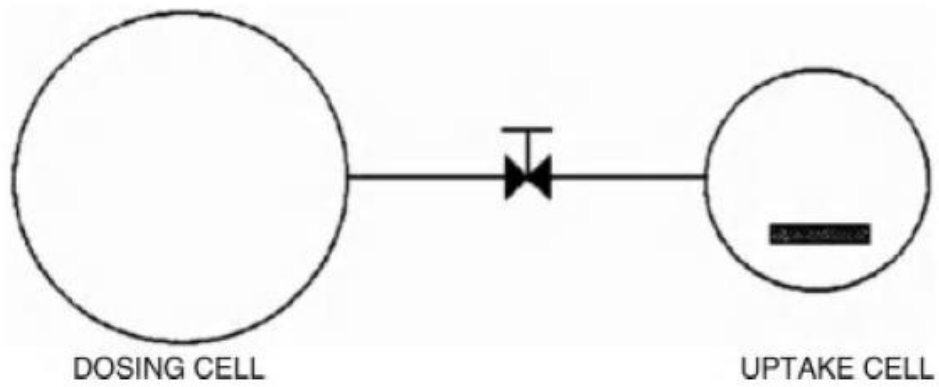

Source: Kärger (2011)

The response curve of a piezometric experiment is a curve of the pressure change in function of time, Figure 2.4; the diffusivity is calculated by correlating the speed of pressure change in time. Brandani (1998) discusses this method as well as its limitations, such as the influence of the restriction of the valve separating the two systems.

Figure 2.4 – Piezometric sorption response curve

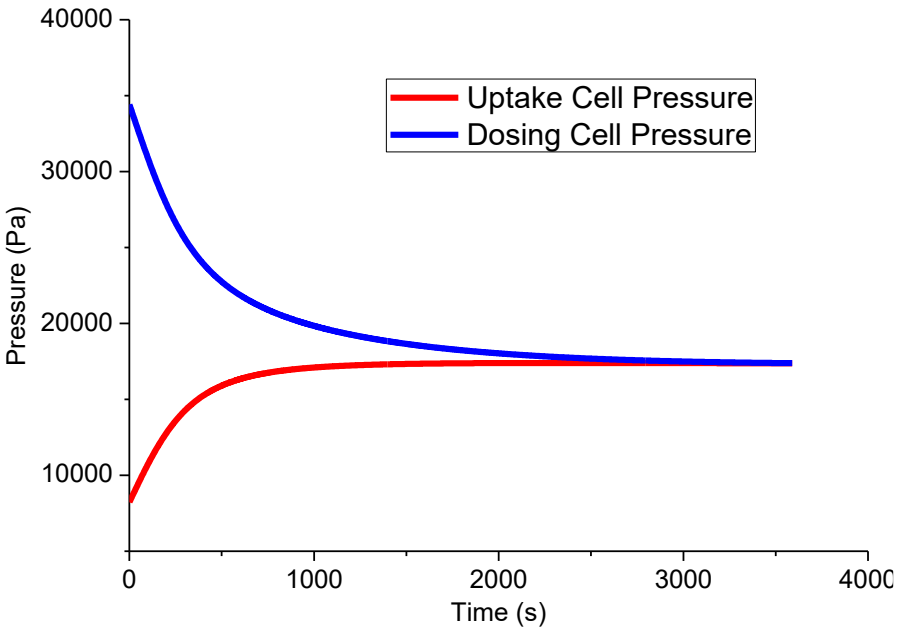

Source : Author

Following the piezometric method, another way of estimating diffusion by the same principle is instead of measuring pressure, using temperature change to calculate the parameters. Grenier *et al.* (1995) derived a non-isothermal model to calculate the diffusivity of systems using a single-step temperature response, Figure 2.5.

Figure 2.5 – Single-step temperature response curve

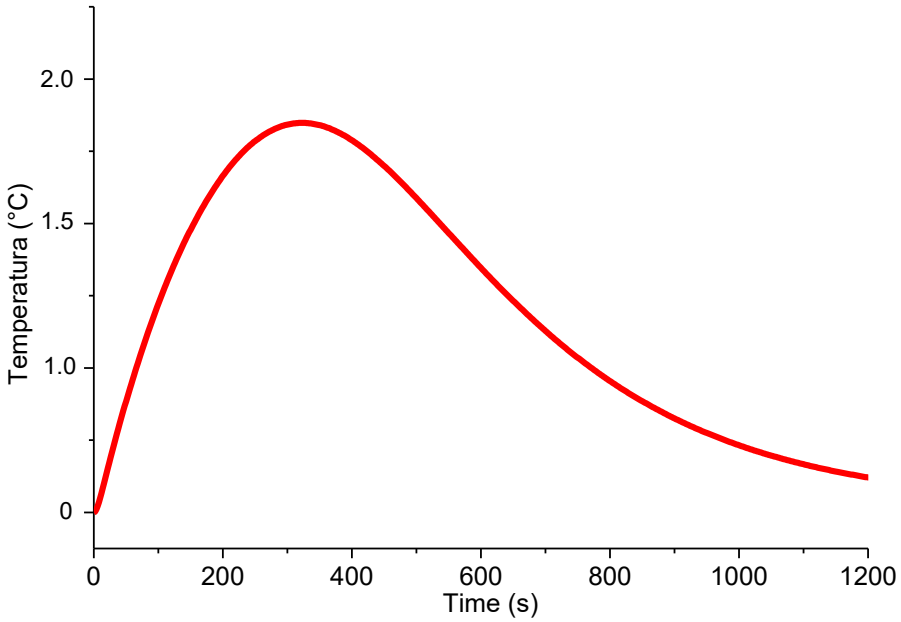

Source: Author

2.2.3 Chromatographic method

This method consists in measuring the diffusivity of a sorbate by flow, either a pulse or a step concentration of adsorbate, through a packed bed of sorbent, Figure 2.6. Chromatography excels in relation to the previous mentioned methods concerning the elimination of external mass transfer restrictions, since the system has a flow of sorbate; the velocity of the fluid reduces the external mass transfer to the particle, making the intraparticle diffusion more significant.

Figure 2.6 – Chromatographic packed bed

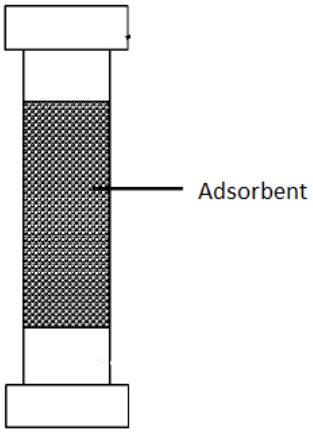

Source : Author

A model, considering constant pressure drop, to represent the flow and adsorption in the column is described by Equation 2.13 and the diffusion coefficients are calculation by applying a model to the rate adsorption term and optimizing the diffusion parameter to the experimental response curve, Figure 2.7.

$$-D_L \frac{\partial^2 c}{\partial z^2} + v\frac{\partial c}{\partial z} + \frac{\partial c}{\partial t} + \left(\frac{1-\epsilon}{\epsilon}\right)\frac{\partial q_{avg}}{\partial t} = 0 \qquad (2.13)$$

Figure 2.7 – Chromatographic response curve, step sorbate concentration

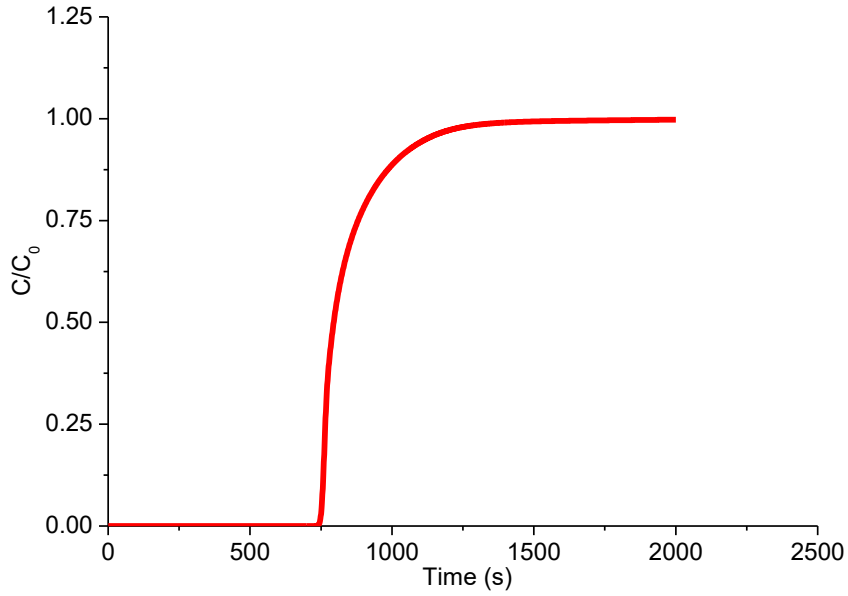

Source : Author

Limitation for the method are the existence of complex flows in the systems that may not be considered in the models, the significance of the pressure drop and heat effects and axial dispersion. Detailed discussion about the resistances have been developed by Haynes (1988).

2.2.4 Zero Length Column Method (ZLC)

ZLC method is a variation of the chromatographic method that was developed to reduce axial dispersion contributions to the system, in order to isolate intraparticle mass transfer and simplify models (Ruthven and Kumar, 1979) (Eic and Ruthven, 1988). A schematic representation of the ZLC experimental setup is shown in Figure 2.8

Figure 2.8 – ZLC experimental Setup

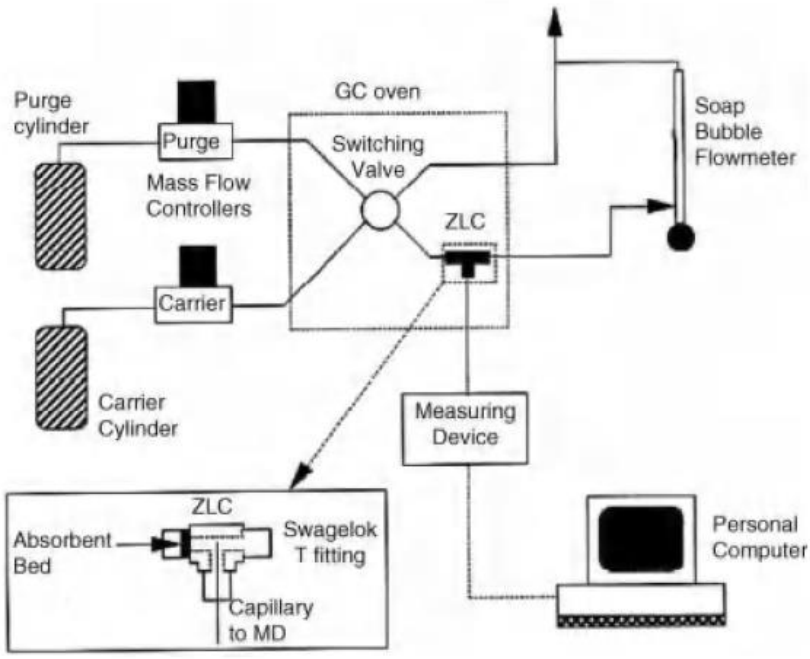

Source : Kärger (2011)

The principle of the method is to use a very small sample of particles to form a bed, the sorbate is initially equilibrated in the system and a desorption is done by a purge with a inert gas. The flow needs to be high enough to maintain an approximately zero concentration at the external surface of the particles. Desorption rate is measured by monitoring effluent composition.

The response curve of a ZLC experiment is one of the ratio of the concentration at a time per the initial concentration, Figure 2.9. A model of intraparticle diffusional control is applied to the system and the diffusivity is calculated by fitting of the parameter. Equation 2.14 shows the result of the mass balances over the system for a fickian diffusion equation, for an adsorption within the limits of Henry Law (Ruthven and Eic, 1988).

Figure 2.9 – ZLC Response curve

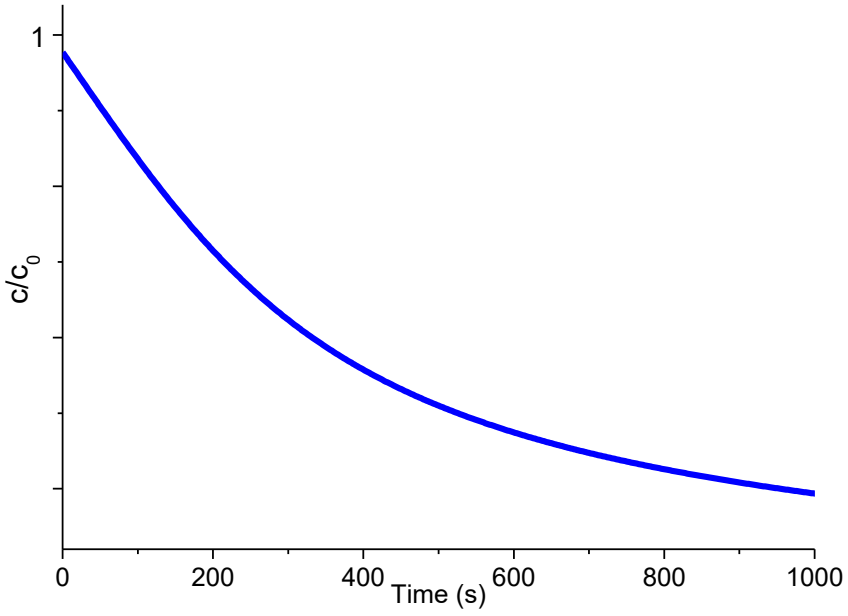

$$\frac{c}{c_0} = 2L \sum_{n=1}^{\infty} \frac{e^{\left(-\frac{\beta_n^2 Dt}{r_c^2}\right)}}{[\beta_n^2 + L(L-1)]} \tag{2.14}$$

Parameters β an L are given by Equation 2.15 and 2.16 below.

$$\beta_n cot\beta_n + L - 1 = 0 \tag{2.15}$$

$$L = \frac{\epsilon v r_c^2}{3(1-\epsilon)K_H Dl} \tag{2.16}$$

2.3 General Microcalorimetry Concepts

Adsorption microcalorimetry is a technique focused on measuring and studying heat effects and parameters of adsorption. Phys sorption is an exothermic process and each sorbate-sorbent system will exhibit a characteristic Enthalpy of Adsorption, which is the result of the

contributions of different intermolecular interactions (Rouquerol *et al.*, 2014). Thus, microcalorimetry is a technique that can be used to characterize porous solids.

Sorption Enthalpy is subjected to variations due to cumulative sorbate loading, in heterogeneous solids, different contributions of sorbate-sorbent and sorbate-sorbate apply, causing different values of Enthalpy as a function of loading, this parameter is known as differential enthalpy, which is also measured in the experiments. The form of the differential enthalpy curve will depend on the relative energy of the sorbate-sorbent and sorbate. Solids with stronger sorbate-sorbent interaction exhibit decreasing enthalpies as a function of loading (Fig. 2.9 (c)) and solids with stronger sorbate-sorbate interactions exhibit increasing enthalpies (Fig. 2.9 (a)). This behavior is demonstrated in Figure 2.9 (Llewellyn and Maruin, 2005).

Figure 2.9 – Differential enthalpy behavior; (a) Sorbate-Sorbate interactions; (b) Homogeneous Sorbent-Sorbate interactions; (c) Heterogeneous Sorbent-Sorbate interactions

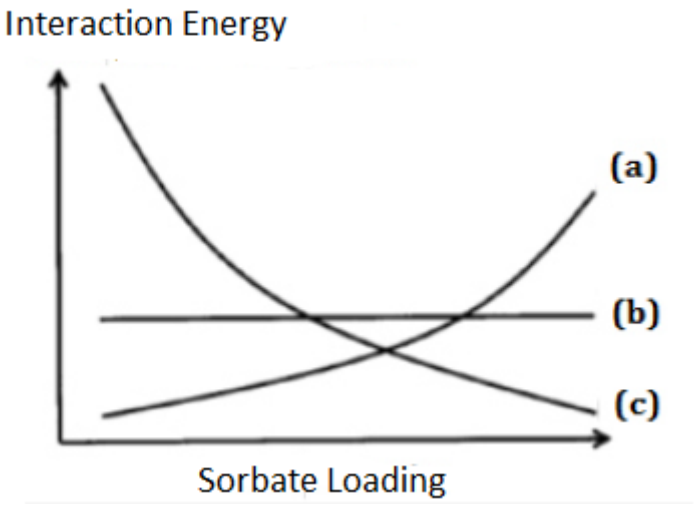

Source : Llewellyn and Maruin (2005)

This behavior is directly correlated with the types of equilibrium isotherms presented above. It is possible to classify each enthalpy behavior according to an isotherm behavior, Figure 2.10.

Figure 2.10 – Differential enthalpy behavior in different isotherm types

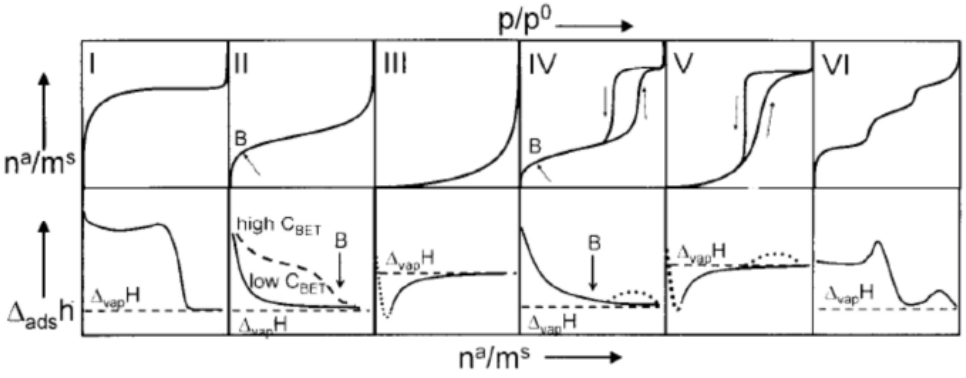

Source : Maia (2014).

Detailed discussion about the theoretical principles and applications can be found in Maia (2014).

3 METHODOLOGY

This section is dedicated to explain the experimental procedures for the measurement of equilibrium and kinetic parameters of adsorption and the derivation of the model used for the same purpose.

3.1 Experimental Apparatus

The experiment setup consists in a Tian-Calvet microcalorimeter (*Setaram* model C80, Caluire, France), show in Figure 3.1, composed internally of an array of thermocouples, coupled with a manometric adsorption setup (Maia *et al.*, 2018) dedicated to perform calorimetric experiments of adsorption of gases. The manometric setup is an arrangement of tubes and valves associated with manometers to accurately set the amount of gas adsorbate for the experiment. Figure 3.2 illustrates the described system.

Figure 3.1 – Tian – Calvet microcalorimeter *Setaram* model C80

Source: Setaram

Figure 3.2 – Experimental setup for the calorimetric experiments

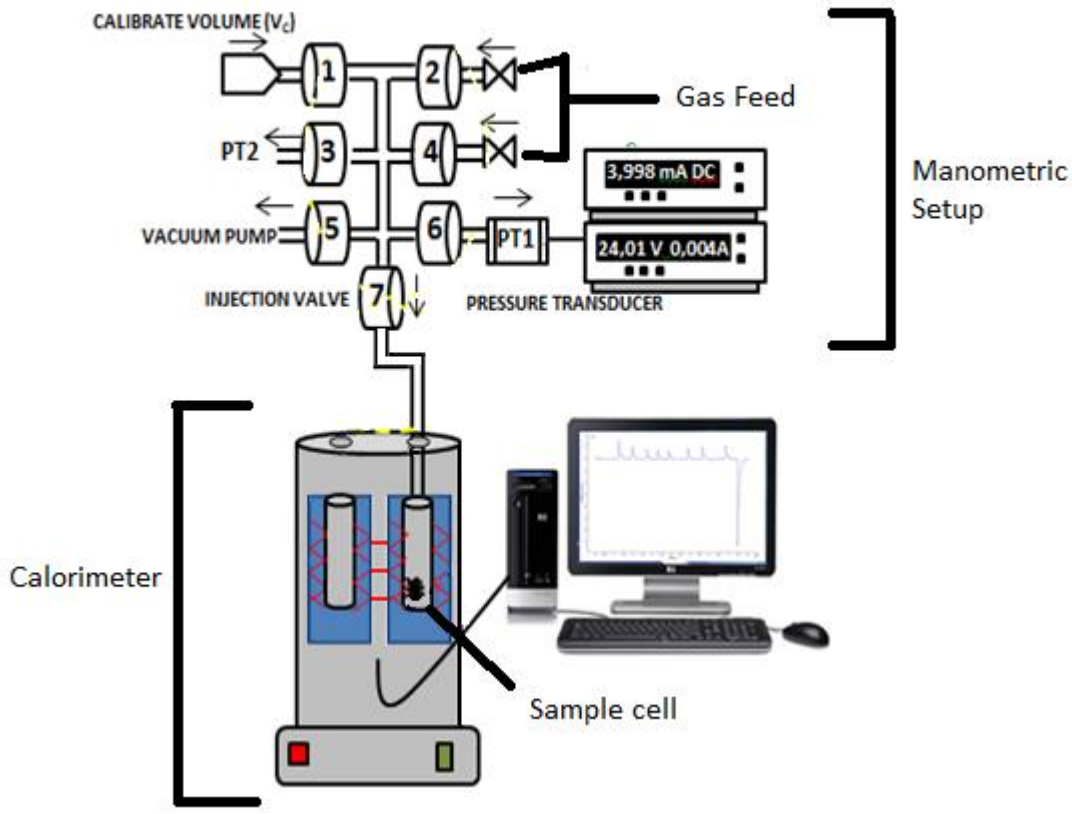

Source: Author

Analyzing Figure 3.2, the space bordered by valves 1 to 7 is occupied by the gas coming from the gas feed. Initially, the system is under high vacuum for the regeneration of the solid, when this step finalizes its schedule, valve 7 is closed, the vacuum is stopped and the gas is inserted

into the dosing vessel through valves 2 or 4. A pressure transducer indicates the quantity of gas inside the domain, when the desired pressure is achieved, valve 7 is opened and the sorbate flows into the calorimeter, where adsorption happens, raising the pressure and generating heat through adsorption, the two systems are kept connected until equilibrium is reached. Thereafter, valve 7 is closed again, a higher quantity of gas is inserted, and the process is repeated. The calorimeter is connected to a computer where the measure of the thermocouples is sent and the heat calculations are made using the Calisto® Software (v1.043 AKTS-Setaram, Caluire, France).

3.1.1 General Experiment description

Initially, the sample undergoes a regeneration process in high vacuum and appropriate high temperatures for each adsorbent compounds, to finish this process the heating of the equipment is turned off and the sample cools until it reaches the ambient controlled temperature of the microcalorimeter. The process is monitored using the before mentioned software reporting temperatures and heat rates, shown in Figure 3.3. When the sample cools and the monitored heat rate stabilizes, the adsorption process can be set up.

Figure 3.3 – Temperature and heat rate reports using software Calisto®.

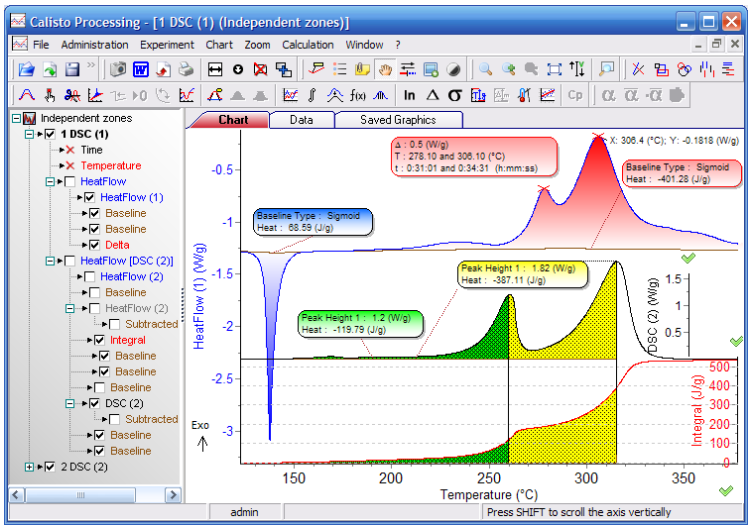

Source: Setaram

To start the calorimetric experiment, the gas is dosed using the manometric setup described before, by setting up a desired pressure, the valve connecting the two systems is opened and the adsorption process happens once the gas reaches the sample. The experiment generates a “microcalorimetric peak” which shows the heat rate, in unis of energy per units of time, in function of time, Figure 3.4.

Figure 3.4 – Microcalorimetric peak as a result of the heat generated by adsorption

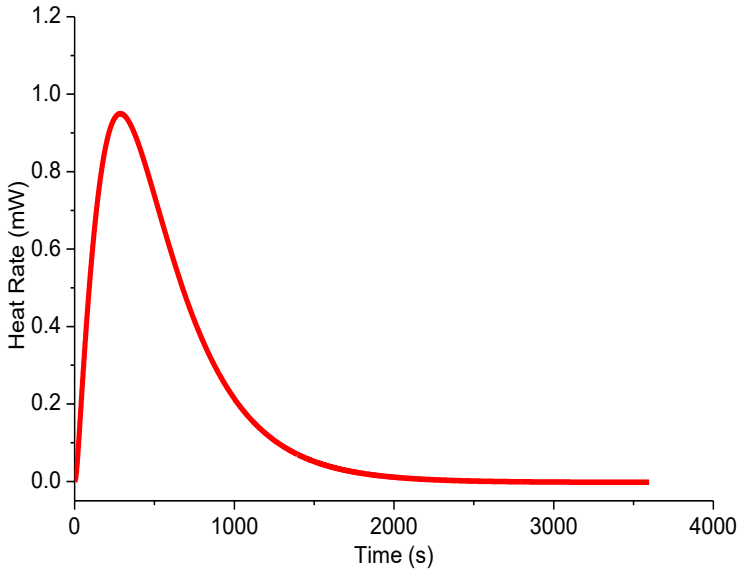

Source: Author

3.2 Measurement of equilibrum properties

Literature reports show that microcalorimetry coupled with the manometric setup is a method suitable for the calculation of adsorption equilibrium properties such as Enthalpies of Adsorption (Rouquerol *et al.*, 1980) and equilibrium isotherms (Rouquerol *et al.*, 1999). This section describes the method for measuring these properties, as they are necessary for the analysis of the kinetics of adsorption.

3.2.1 Equilibrium isotherms determination

The method for obtaining adsorption isotherms is described as the discontinuous procedure (Rouquerol *et al.*, 2014). In a given pressure and temperature on the microcalorimetric cell, it is possible to identify multiple equilibrium points by checking the

stabilization of the baseline, if the baseline is stable in a given value reporting no heat being transferred, this condition of temperature and pressure is an equilibrium point. By introducing a new quantity of adsorbent on the system, the calorimetric peak will be generated, showing heat transfer until the baseline stabilizes again, classifying another equilibrium point at a higher pressure, Figures 3.5 and 3.6.

Figure 3.5 - Equilibrium points by heat rate baseline stabilization.

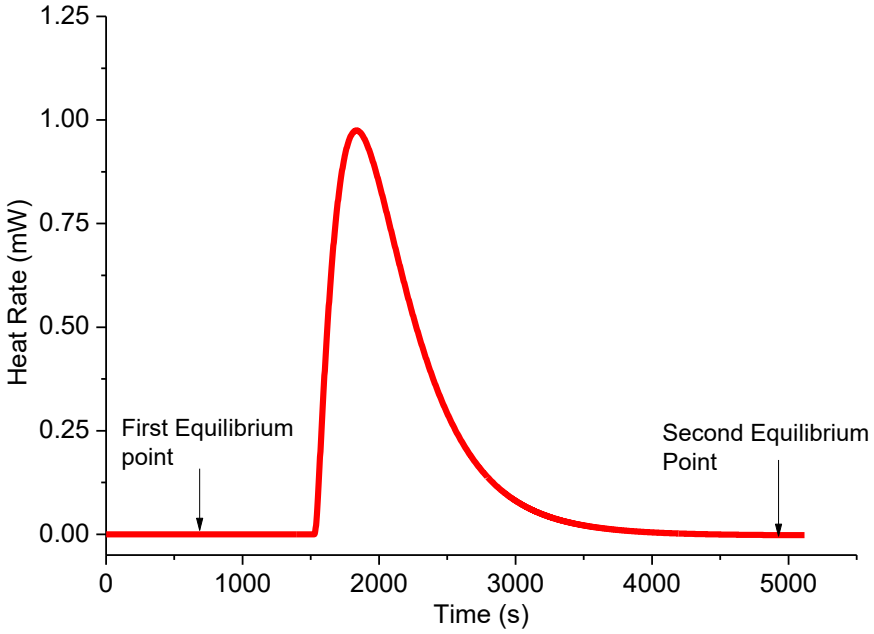

Source: Author

Figure 3.6 – Equilibrium points by pressure stabilization.

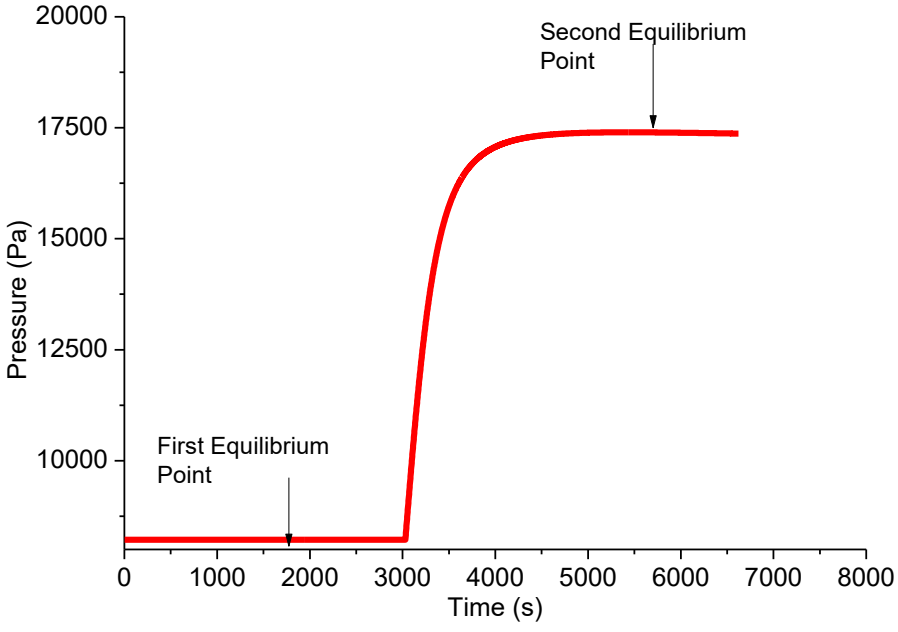

Source: Author

The total and the adsorbed number of moles of gases can be calculated by the measured PVT data, an appropriate equation of state and mass balances between the two equilibrium points. The mass balance for the system can be done by dividing the equipment into three domains: The dosing vessel, where the gas pressure is set up for the adsorption; The microcalorimetric cell, where the gas is adsorbed and the transfer line, which connects the two previous system. Each domain has a constant volume, V_1 for the dosing vessel, V_2 for the transfer line, and V_3 for the calorimetric cell. Figure 3.7 illustrates the division of the domains.

Figure 3.7 – Domain division of the calorimeter

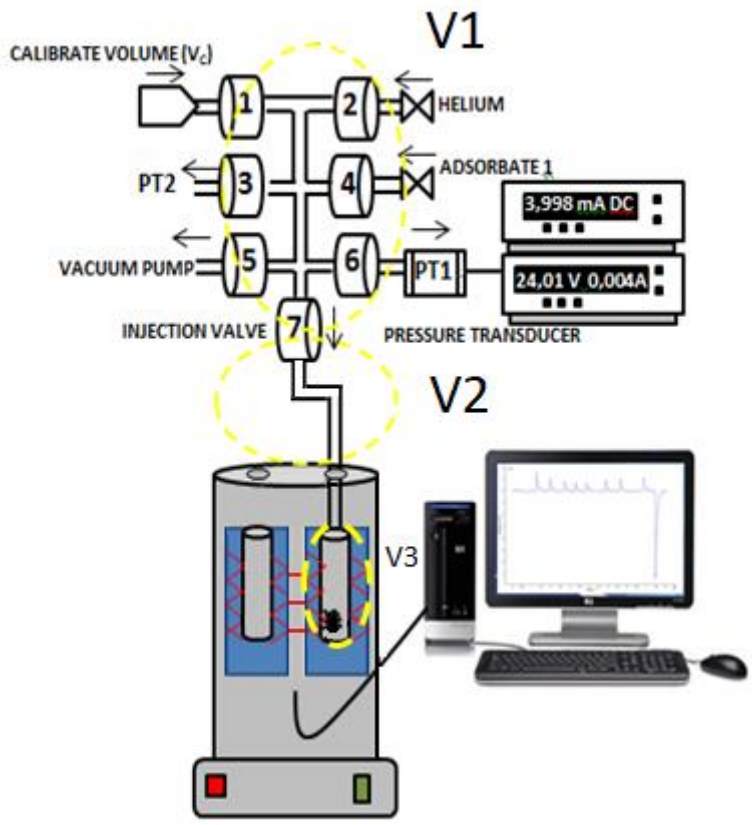

Source: Author

Applying a material balance between two equilibrium points, equation 3.1 is obtained.

$$n_1^I + n_2^I + n_3^I + n_{ads}^I = n_1^{II} + n_2^{II} + n_3^{II} + n_{ads}^{II} \quad (3.1)$$

The first assumption for the system is that the gas can be described through the Ideal Gas Law, the assumption holds in low pressures and, for this work, the experimental pressures employed are all inferior to 1 bar, thus, Equation 3.1 can be rewritten as Equation 3.2.

$$\Delta n_{ads} = \frac{1}{R_g T}\left((P_1^I - P_1^{II})V_1 + (P_2^I - P_2^{II})V_2 + (P_3^I - P_3^{II})V_3\right) \tag{3.2}$$

The second assumption is that the pressure in the transfer line is equal to the pressure in the microcalometric cell, this assumption holds by analyzing Figure 3.7, the dosing vessel is sealed form the two other domains by valve 7, and the transfer line and the cell are continuously connected, so $P_2 = P_3$, Equation 3.2 turns into Equation 3.3.

$$\Delta n_{ads} = \frac{1}{R_g T}\left((P_1^I - P_1^{II})V_1 + (P_3^I - P_3^{II})(V_2 + V_3)\right) \tag{3.3}$$

Finally, since the system equilibrates, the final pressures of the dosing vessel and calorimetric cell must be the same, thus $P_1^{II} = P_3^{II} = P_E$, forming Equation 3.4.

$$\Delta n_{ads} = \frac{1}{R_g T}\left(-P_E(V_1 + V_2 + V_3) + P_1^I V_1 + P_3^I (V_2 + V_3)\right) \tag{3.4}$$

The pressures are continuously measured in the system, so their values are given, but there are still three parameters left to solve the equation, the three volumes, these volumes can be obtaining by performing an experiment without the adsorbent in the calorimetric cell or with an inert gas, a blank experiment.

3.2.2 Blank Experiments

The blank experiments are set up in the same way as an adsorption experiment, the volumes can be calculated by setting up an experiment where no adsorption happens, this is achieved either by expanding the adsorbate gas into the cell when there is no adsorbent, or by expanding an inert gas into the cell with the adsorbent in. The difference between these two is that the volume calculated by the expansion without sample is slightly higher than with the inert gas due to solid particles volume, in this work the expansions are done with the inert gas Helium for better accuracy.

Applying Equation 3.4 on the system without adsorption, the term Δn_{ads} is zero, so the material balance for the new system is written in the form of Equation 3.5.

$$\frac{V_1}{V_2 + V_3} = \frac{P_E - P_3^I}{P_1^I - P_E} \tag{3.5}$$

The volume of the dosing vessel is calculated by calibration. With a given value of V_1 it is possible to calculate the sum $V_2 + V_3$ and with this value the adsorbed number of moles can be calculated. It is important to note that, for isotherm calculations, it is not necessary to obtain the individual values of V_2 and V_3, as shown in Equations 3.4 and 3.5, but the blank calorimetric experiment provides heat transfer data for the calculation of these volumes by applying energy balances to the system.

The heat rate as a function of time, Figure 3.5, reported by the calorimeter software can be integrated to calculate the total heat transferred by the experiment, so by calculating the area below the microcalorimetric peak, the total heat Q_{tot} is obtained, Figure 3.8 and Equation 3.6.

Figure 3.8 – Integration of the microcalorimetric peak

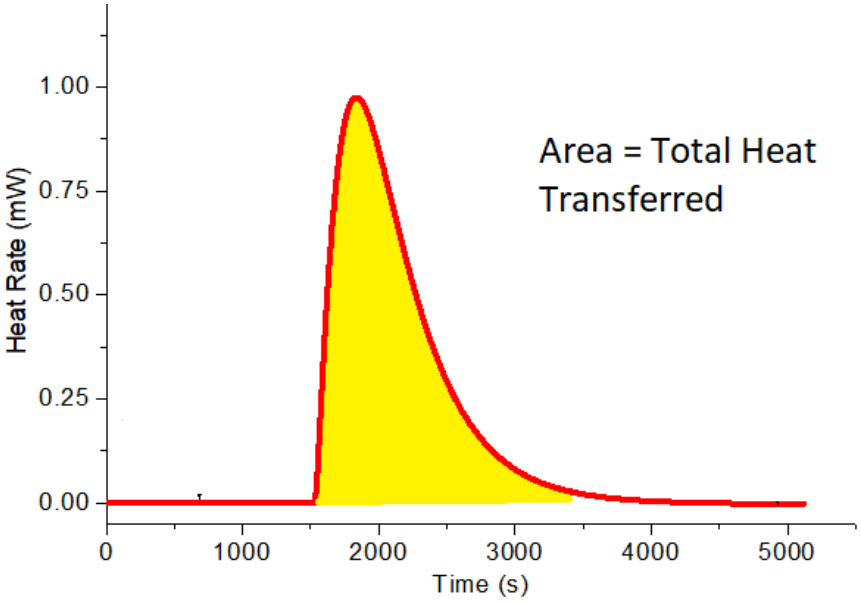

Source: Author

$$Q_{tot} = \int_0^{\infty} \dot{Q}(t)dt \tag{3.6}$$

With this information, it is possible to obtain further parameters of the experiment through energy balance in the microcalorimetric cell, domain of volume V_3. The domain of the cell is an open system with heat transfer, the energy balance is represented by Equation 3.7.

$$\frac{dU}{dt} = \dot{Q} + \dot{W}_s + \dot{n_{in}}\widehat{H_{in}} \tag{3.7}$$

Integrating Equation 3.7 with respect to times $t = 0$ and $t \to \infty$, and applying isothermal conditions, $\frac{dU}{dt} = 0$ and eliminating axis work yields equation 3.8.

$$0 = \int_0^\infty \dot{Q}(t)dt + \int_0^\infty \dot{n_{in}}\widehat{H_{in}}\, dt \tag{3.8}$$

Combining Equations 3.6 and 3.8, and expanding the specific enthalpy term as a function of internal energy yields Equation 3.9.

$$0 = Q_{tot} + \int_0^\infty \dot{n_{in}}\widehat{U_{in}}\, dt + \int_0^\infty P_3\dot{V}_3\, dt \tag{3.9}$$

Solving the integrals from Equation 3.9 considering constant volume for the cell and isothermal conditions, the final form for the energy balance is shown in Equation 3.10.

$$V_3 = -\frac{Q_{tot}}{P_E - P_3^I} \tag{3.10}$$

The previous equation shows that the volume of the microcalorimetric cell is the value of the area below the microcalorimetric curve divided by the change in pressure in the blank experiment, with all these parameters, the equilibrium isotherm of the adsorbate-adsorbent system can be fully determined.

3.2.3 Measurement of the Enthalpy of Adsorption

The discontinuous procedure for calorimetry described in the previous sections is able to measure the differential Enthalpy of Adsorption, which is the Enthalpy of Adsorption as a function of the equilibrium adsorbed quantity. The curve of the differential enthalpy for the interaction of adsorbates with heterogeneous adsorbents is shown in Figure 3.9. (Llewellyn and Maruin, 2005). Most adsorbents are heterogeneous, so the curves that are obtained through

microcalorimetry are mostly in the form of the curve of Figure 3.9, which applies to the samples studied in this work.

Figure 3.9 – Differential Enthalpy of adsorption for heterogeneous adsorbents

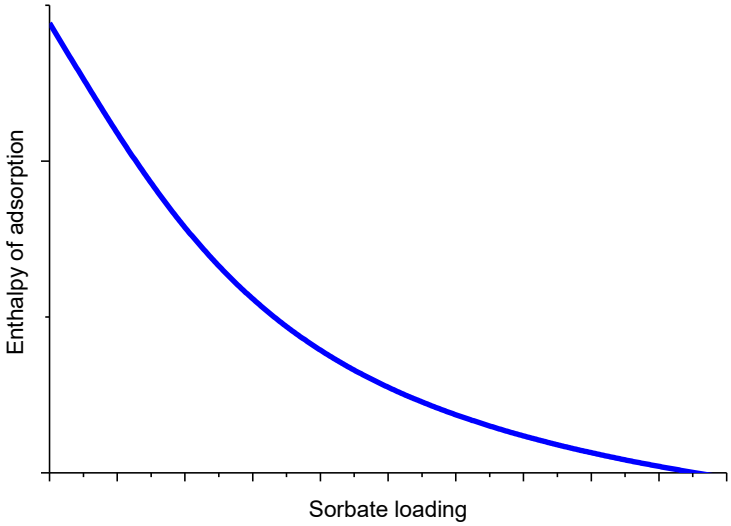

Source: Author

The procedure for calculating the Enthalpy of adsorption is applying an energy balance to the system, similar to Equation 3.8 but with the addition of the adsorption energy, which yields Equation 3.11.

$$0 = \int_0^{\infty} \dot{Q}(t)dt + \int_0^{\infty} \dot{n_{in}}\widehat{H_{in}}\, dt - \Delta n_{ads}\Delta H_{ads} \tag{3.11}$$

Isolating the Enthalpy of adsorption term, equation 3.12 is obtained.

$$\Delta H_{ads} = \frac{-Q_{tot}}{\Delta n_{ads}} - \frac{(P_E - P_3^I)V_3}{\Delta n_{ads}} \tag{3.12}$$

Equation 3.12 can be rearranged to show that the total heat of the experiment is the sum of the heat due to compression and the heat of adsorption. With the area of the peak, the measured pressures, the calculated volume through the blank experiments and the adsorption isotherm, the differential enthalpy curve can be obtained in the discontinuous procedure.

3.3 Measurement of kinetic properties

The principle of measuring kinetic parameters of adsorption through calorimetry is that the rate of heat generated in the phenomena is proportional to the rate of mass transfer (Grenier *et al.*, 1994). A process with a relatively fast mass transfer will generate heat quickly and will reach equilibrium quickly. In a microcalorimetric experiment, this effect can be seen through the microcalorimetric peaks, considering a process with the same energy output, a fast mass transfer will generate sharp peaks with relatively short time duration, and slow mass transfer will generate short peaks with relatively long duration, Figure 3.10.

Figure 3.10 – Fast and slow mass transfer process seen through the microcalorimetric peaks

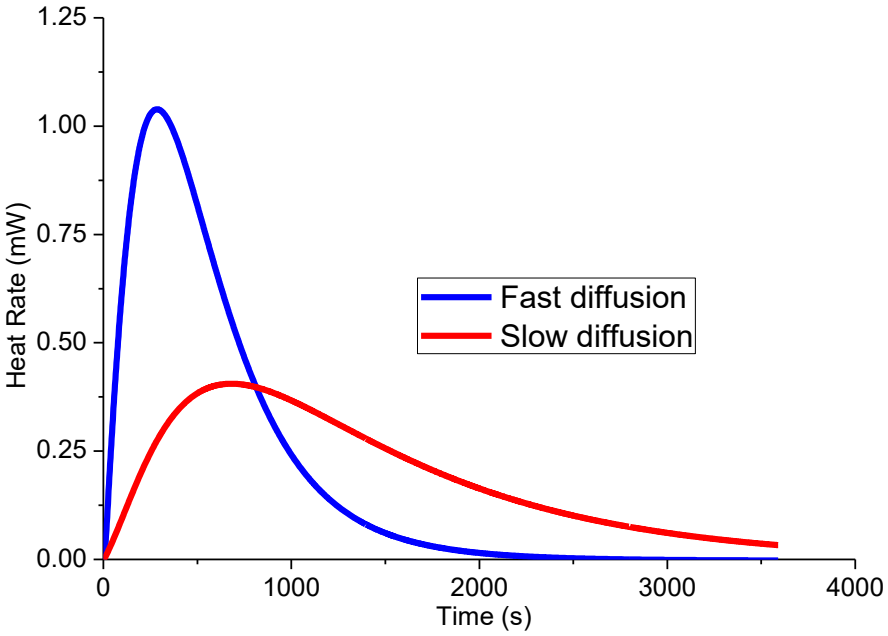

Source: Author

The rate of heat generation in a system can be written in the form of Equation 3.13

$$\frac{dQ_{ads}}{dt} = m_s \, \Delta H_{ads} \frac{d\overline{q}}{dt} \tag{3.13}$$

To calculate the mass transfer parameters, it is necessary to employ an appropriate model to describe de adsorption rate term, $\frac{d\overline{q}}{dt}$.

3.3.1 Linear Driving Force model.

Glueckauf (1955) proposed the simple Linear Driving Force (LDF) model for the mass transfer rate of an adsorption process, the equation for the mass transfer rate is shown in Equation 3.14.

$$\frac{d\overline{q}}{dt} = k_{LDF}(q_E - \overline{q}) \tag{3.14}$$

This model has the advantage of being a simple linear model, providing simpler analytical and numerical solutions when applied to adsorption systems. The constant k_{LDF} can be expanded so that it combines all diffusional processes that may happen in a given process, Equation 3.15.

$$\frac{1}{k_{LDF}K} = \frac{3}{R_p k_f} + \frac{R_p^2}{15\epsilon_p D_p} + \frac{r_c^2}{15D_c} \tag{3.15}$$

The above expansion shows that the linear driving force constant contains the three possible types of mass transfer resistances in an adsorption process, external film diffusion resistance, macropore diffusion resistance and intracrystalline diffusion resistance. Thus, the linear model is useful when dealing with system where more than one resistance is significant (Raghavan and Ruthven, 1985), such as systems with activated carbons and pelletized adsorbent crystals.

3.3.2 Intraparticle diffusion model

This work focuses on the study of microporous materials such as zeolites for the measurement of kinetic parameters, in these materials, the rate of mass transfer is controlled by the micropore intracrystalline diffusion. The model for the diffusion in the micropores of a spherical particle is shown in Equation 3.16. If the model is used in a system where multiple resistances take place, the diffusion term should be the effective diffusivity, D_{eff}

$$\frac{\partial q}{\partial t} = \frac{1}{r^2}\frac{\partial}{\partial r}\left(r^2 D_c \frac{\partial q}{\partial r}\right) \tag{3.16}$$

If the experiment is conducted in a range, where there is a small change in adsorbed quantity, which is valid for the discontinuous procedure described in this work, Equation 3.16 can be written in the form of Equation 3.17 below.

$$\frac{\partial q}{dt} = D_c\left(\frac{\partial^2 q}{\partial r^2} + \frac{2}{r}\frac{\partial q}{\partial r}\right) \tag{3.17}$$

The domain of the equation holds for $0 < r < r_c$ which has the following boundary and initial conditions

$$q(r,0) = q_0 = q_E(P_3^I)\rho_p \;\; \forall\, r \tag{3.18}$$

$$\frac{\partial q}{\partial r}(0,t) = 0;\, q(r_c,t) = q_E(P_3(t))\rho_p \tag{3.19}$$

It is possible to write Equation 3.17 as a function of non-dimensional radius $\frac{r}{r_c} = r_a$, yielding Equation 3.20.

$$\frac{\partial q}{dt} = \frac{D_c}{r_c^2}\left(\frac{\partial^2 q}{\partial r_a^2} + \frac{2}{r_a}\frac{\partial q}{\partial r_a}\right) \tag{3.20}$$

This modification makes the boundary conditions now hold for $0 < r_a < 1$, this form of the equation is useful when there is no data for the crystal radius r_c, so the parameter calculated in the diffusion experiment is the diffusional time constant, $\frac{D_c}{r_c^2}$. The diffusion coefficient can be considered constant if the equilibrium isotherm is within Henry law conditions, but if the isotherm is near saturation, it is necessary to employ Darken's correction (Darken, 1948), Equation 3.21.

$$D_c = D_{c0}\frac{dlnP_E}{dlnq} \tag{3.21}$$

3.3.3 Measuring mass transfer parameters through adsorption calorimetry

The experimental setup for the experiment focused on measuring mass transfer is the same as for the measurement of equilibrium properties; the difference for the kinetics is that the material and energy balances are dynamic. The full model derivation will follow by considering the same domain division of Figure 3.7 and considering the following assumptions.

- Heat is transferred from the gas to tubing in the dosing cell and transfer line by convection; in both cases, external temperature is constant;
- Pressure in the transfer line is equal to that in the dosing cell at any time;
- The temperature of the adsorbent and the adsorbed phase are the same as the temperature of the gas in the dosing cell at any time;
- The ideal gas law is the considered Equation of State for the employed gases in the pressure and temperature ranges under study;
- Adsorbent samples are considered spherical (in the homogeneous diffusion model);
- External (film) mass transfer resistances are negligible.

The generic form for the dynamic material balance for the three domains is described according to Equation 3.22

$$Rate\ of\ mass\ change = Gas\ Inlet - Gas\ outlet + Rate\ of\ mass\ transfer \tag{3.22}$$

3.3.3.1 Dosing Vessel Material Balance

For the dosing vessel of volume V_1 , each term of the previous equation are shown below

$$Rate\ of\ mass\ change = \frac{dC_1}{dt}V_1 \tag{3.23}$$

$$Gas\ inlet = 0 \tag{3.24}$$

$$Gas\ outlet = n_{out} \tag{3.25}$$

$$Rate\ of\ mass\ transfer = 0 \tag{3.26}$$

Which yields Equation 3.27

$$\frac{dC_1}{dt}V_1 = -n_{out} \tag{3.27}$$

3.3.3.2 Transfer line Material Balance

For the transfer line of volume V_2 , each term of Equation 3.22 are shown below

$$Rate\ of\ mass\ change = \frac{dC_2}{dt}V_2 \tag{3.28}$$

$$Gas\ inlet = n_{out} \tag{3.29}$$

$$Gas\ outlet = n_{in} \tag{3.30}$$

$$Rate\ of\ mass\ transfer = 0 \tag{3.31}$$

Which yields Equation 3.32

$$\frac{dC_2}{dt}V_2 = n_{out} - n_{in} \tag{3.32}$$

3.3.3.3 Calorimetric Cell Material Balance

For the microcalorimetric cell of volume V_3 , each term of Equation 3.22 are shown below

$$Rate\ of\ mass\ change = \frac{dC_3}{dt}V_3 \tag{3.33}$$

$$Gas\ inlet = n_{in} \tag{3.34}$$

$$Gas\ outlet = 0 \tag{3.35}$$

$$Rate\ of\ mass\ transfer = -m_s\frac{d\overline{q}}{dt} \tag{3.36}$$

Which yields Equation 3.37.

$$\frac{dC_3}{dt}V_3 = n_{in} - m_s\frac{d\overline{q}}{dt} \tag{3.37}$$

Finally, the full set of equations for the material balance as well as the ideal gas law applied to each domain, Equations 3.38 to 3.43 are organized below.

$$\frac{dC_1}{dt}V_1 = -n_{out} \tag{3.38}$$

$$\frac{dC_2}{dt}V_2 = n_{out} - n_{in} \tag{3.39}$$

$$\frac{dC_3}{dt}V_3 = n_{in} - m_s\frac{dq}{dt} \tag{3.40}$$

$$P_1 = C_1 R_g T_1 \tag{3.41}$$

$$P_2 = C_2 R_g T_2 \tag{3.42}$$

$$P_3 = C_3 R_g T_3 \tag{3.43}$$

As described in the experimental section, the pressures of the dosing vessel and the sample cell are continuously measured and their values will reach equilibrium over the span of the experiment, as Figure 3.11 shows. For the system of equations to be well posed, one of those two pressures needs to be described as an equation in function of time. Due to a delay in the response of pressure P_3 when the experiment starts, pressure P_1 is chosen to be adjusted by an exponential behavior described by Equation 3.44.

Figure 3.11 – Pressure profiles during the microcalorimetry experiment.

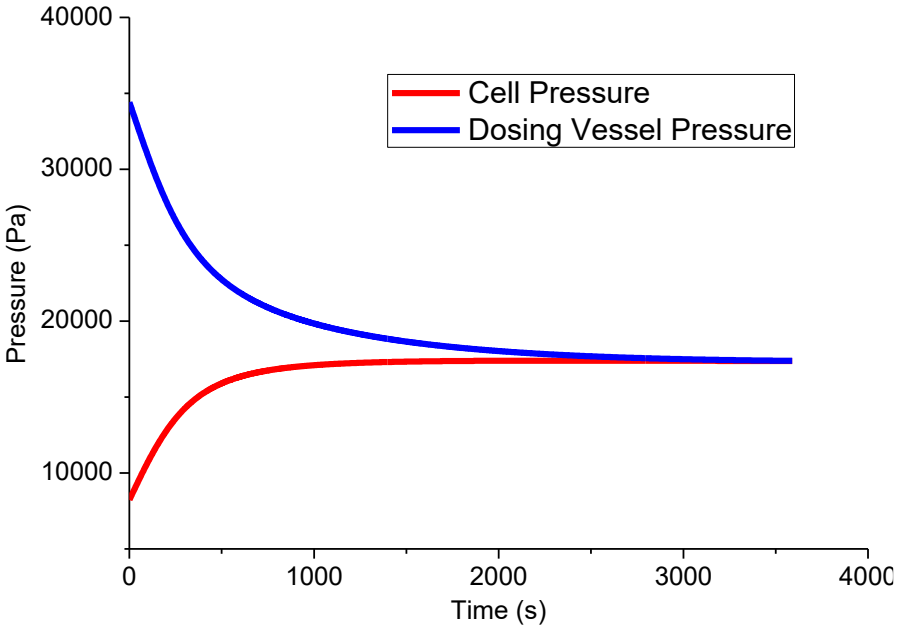

Source: Author

$$P_1(t) = P_E + (P_1^I - P_E)e^{-\alpha t} \tag{3.44}$$

To describe the energy dynamics of the system, an energy balance is also applied in the same way the material balance was applied to the three domains, Equation 3.45 shows the general form for the energy balance.

$$\begin{aligned} &Rate\ of\ change\ of\ energy \\ &\quad = Heat\ transferred\ from\ the\ gas\ flux \\ &\quad + Heat\ transferred\ from\ convection \\ &\quad + Heat\ transferred\ \ from\ adsorption \\ &\quad + Heat\ from\ pressure\ change \end{aligned} \tag{3.45}$$

3.3.3.4 Dosing Vessel Energy Balance

For the dosing vessel of volume V_1 , each term of the previous equation are shown below

$$Rate\ of\ change\ of\ energy = C_1 c_v \frac{dT_1}{dt} V_1 + m_w c_{pw} \frac{dT_1}{dt} \tag{3.46}$$

$$Heat\ transferred\ from\ the\ gas\ flux = 0 \tag{3.47}$$

$$Heat\ transferred\ from\ convection = h_1 A_1 (T_{o1} - T_1) \tag{3.48}$$

$$Heat\ transferred\ \ from\ adsorption = 0 \tag{3.49}$$

$$Heat\ from\ pressure\ change = \frac{d}{dt}\left(\frac{P_1}{T_1}\right)T_1V_1 \tag{3.50}$$

Which yields Equation 3.51.

$$C_1c_v\frac{dT_1}{dt}V_1 + m_wc_{pw}\frac{dT_1}{dt} = \frac{d}{dt}\left(\frac{P_1}{T_1}\right)T_1V_1 + h_1A_1(T_{o1} - T_1) \tag{3.51}$$

3.3.3.5 Transfer Line Energy Balance

For the transfer line of volume V_2 , each term of Equation 3.42 are shown below

$$Rate\ of\ change\ of\ energy = C_2c_v\frac{dT_2}{dt}V_2 + m_wc_{pw}\frac{dT_2}{dt} \tag{3.52}$$

$$Heat\ transferred\ from\ the\ gas\ flux = \dot{n}_{out}c_v(T_1 - T_2) \tag{3.53}$$

$$Heat\ transferred\ from\ convection = h_2A_2(T_{o1} - T_2) \tag{3.54}$$

$$Heat\ transferred\ \ from\ adsorption = 0 \tag{3.55}$$

$$Heat\ from\ pressure\ change = \frac{d}{dt}\left(\frac{P_2}{T_2}\right)T_2V_2 \tag{3.56}$$

Which yields Equation 3.57.

$$C_2c_v\frac{dT_2}{dt}V_2 + m_wc_{pw}\frac{dT_2}{dt} = \dot{n}_{out}c_v(T_1 - T_2) + \frac{d}{dt}\left(\frac{P_2}{T_2}\right)T_2V_2 + h_2A_2(T_{o1} - T_2) \tag{3.57}$$

3.3.3.6 Microcalorimetric cell Energy Balance

For the microcalorimetric cell of volume V_3 , each term of Equation 3.42 are shown below

$$Rate\ of\ change\ of\ energy = C_3c_v\frac{dT_3}{dt}V_3 + m_sc_{ps}\frac{dT_3}{dt} + m_sc_v\bar{q}\frac{dT_3}{dt} \tag{3.58}$$

$$Heat\ transferred\ from\ the\ gas\ flux = \dot{n}_{in}c_v(T_2 - T_3) \tag{3.59}$$

$$Heat\ transferred\ from\ convection = h_3A_3(T_c - T_3) \tag{3.60}$$

$$Heat\ transferred\ \ from\ adsorption = m_s\frac{d\bar{q}}{dt}(-\Delta H_{ads}) \tag{3.61}$$

$$Heat\ from\ pressure\ change = \frac{d}{dt}\left(\frac{P_3}{T_3}\right)T_3V_3 \tag{3.62}$$

Which yields Equation 3.63.

$$\begin{aligned} C_3c_v\frac{dT_3}{dt}V_3 + m_sc_{ps}\frac{dT_3}{dt} + m_sc_v\bar{q}\frac{dT_3}{dt} = \\ = \dot{n}_{in}c_v(T_2 - T_3) + \frac{d}{dt}\left(\frac{P_3}{T_3}\right)T_3V_3 + h_3A_3(T_{cw} - T_3) \\ + m_s\frac{d\bar{q}}{dt}(-\Delta H_{ads}) \end{aligned} \tag{3.63}$$

Finally, the full set of equations for the energy balance, Equation 3.64, 3.65 and 3.66 is organized below.

$$C_1c_v\frac{dT_1}{dt}V_1 + m_wc_{pw}\frac{dT_1}{dt} = \frac{d}{dt}\left(\frac{P_2}{T_2}\right)T_2V_2 + h_1A_1(T_{o1} - T_1) \tag{3.64}$$

$$\begin{aligned} C_2c_v\frac{dT_2}{dt}V_2 + m_wc_{pw}\frac{dT_2}{dt} \\ = \dot{n}_{out}c_v(T_1 - T_2) + \frac{d}{dt}\left(\frac{P_2}{T_2}\right)T_2V_2 + h_2A_2(T_{o1} - T_2) \end{aligned} \tag{3.65}$$

$$\begin{aligned} C_3c_v\frac{dT_3}{dt}V_3 + m_sc_{ps}\frac{dT_3}{dt} + m_sc_v\bar{q}\frac{dT_3}{dt} = n_{in}c_v(T_2 - T_3) + \frac{d}{dt}\left(\frac{P_3}{T_3}\right)T_3V_3 \\ + h_3A_3(T_{cw} - T_3) + m_s\frac{d\bar{q}}{dt}(-\Delta H_{ads}) \end{aligned} \tag{3.66}$$

The derived model represents the material and energy exchanges that happen on the interior parts of the domains, but the detection of the heat rates by the thermocouples is made outside the walls of the calorimetric cell, thus it is necessary to apply a heat transfer model for microcalorimetric cell wall.

It is important to point out that the terms related to the energy induced by pressure change, Equations 3.50, 3.56 and 3.62 can be simplified to a pure $\frac{dP}{dt}V$ form, if the temperature change is small, which is the case for the experiments taken in this work.

Figure 3.12 illustrates the heat conduction through the cell wall, heat is transferred by convection to the cell wall and is conducted until it reaches the thermocouples located at the cell wall outer radius, where the measurement of the microcalorimetric peak takes place, from there, heat is conducted until it reaches the calorimeter wall, which has a controlled temperature.

Figure 3.12 – Representation of the heat transfer domains on the microcalorimetric cell wall

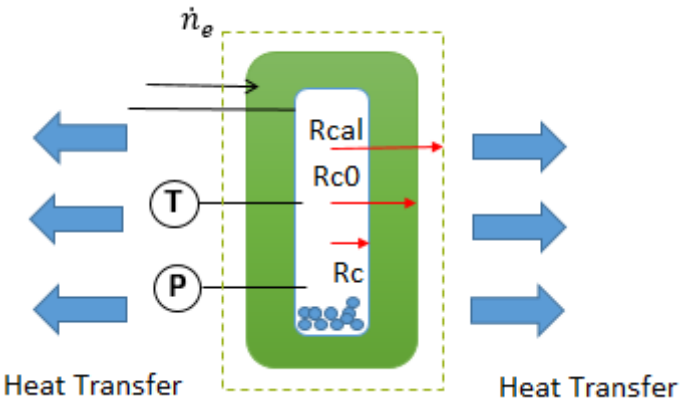

Source: Author

The heat conduction is assumed to occur only in the radial direction and is described through the transient heat conduction model, Equation 3.67

$$\rho_{cw} c_{cw} \frac{dT_{cw}}{dt} = \frac{1}{r_{cw}} k_{cw} \left(\frac{\partial}{\partial r_{cw}} \left(r_{cw} \frac{\partial T_{cw}}{\partial r_{cw}} \right) \right) \tag{3.67}$$

The previous equation holds for $R_{cw} < r_{cw} < R_{cw0}$.

After the model equations are posed, proper initial and boundary condition are to be assigned, below is listed the initial conditions applied to the model, excluding the cell wall conduction

$$P_3(t = 0) = P_3^I \tag{3.68}$$

$$\overline{q}(t = 0) = q_{E0} \tag{3.69}$$

$$T_1(t = 0) = T_{o1} \tag{3.70}$$

$$T_2(t = 0) = T_{o1} \tag{3.71}$$

$$T_3(t = 0) = T_{o2} \tag{3.72}$$

For the heat conduction on the cell wall, the following equations apply

$$-k_{cw} A_3 \frac{\partial T_{cw}}{\partial r_{cw}} (r_{cw} = R_{cw}, t) = - h_3 A_3 (T_{cw} - T_3) \tag{3.73}$$

$$T_{cw}(r_{cw}, t = 0) = T_{o2} \tag{3.74}$$

$$-k_{cw}A_{cw0}\frac{\partial T_{cw}}{\partial r_{cw}}(r_{cw}=R_{cw0},t)=-K(T_{o2}-T_{cw}) \quad (3.75)$$

Equation 3.75 is made to represent the actual measure of the equipment, it measures the heat rate from the phenomena as a function of a calibration constant multiplied by the temperature difference.

The demonstrated model is valid when performing a regular calorimetric experiment, so in one experiment it is possible to obtain both equilibrium and kinetic parameters, but the mass transfer process can also be modelled using calorimetric desorption, which will be discussed further.

3.3.4 Measuring mass transfer parameters through desorption calorimetry

The measurement of kinetic parameters can also be done using the compound desorption in the microcalorimeter, further analysis of using this method show that the desorption model is simpler in comparison to the adsorption model, although the former needs an additional experiment for the determination of both equilibrium and kinetic parameters.

The experimental setup for the desorption is slightly different. First, the adsorbent is saturated with the adsorbate until it reaches pressures in the range of 1 bar. The dosing vessel is evacuated using the vacuum pump so that it remains in a low pressure. The experiment then is performed in a reversed way, valve seven from figure is opened and the gas flows from the higher-pressure microcalorimetric cell wall to the lower-pressure dosing cell. The output of the microcalorimetric peaks in the used software for the desorption experiment is illustrated in Figure 3.13.

Figure 3.13 – Output of the desorption experiment.

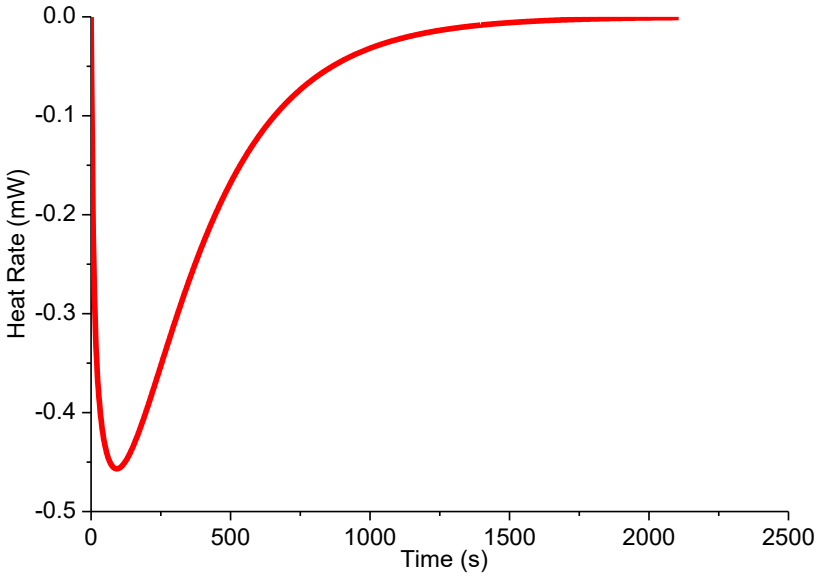

Source: Author

The dynamic model for the described experiment has the same assumptions of the regular adsorption one, but for the new case, the domains of the model can be limited to only the microcalorimetric cell wall, which is modelled in the same way the dosing vessel is modelled in the previous model, as a constant volume domain that discharges into another. Figure 3.14.

Figure 3.14 – Microcalorimetric cell model representation

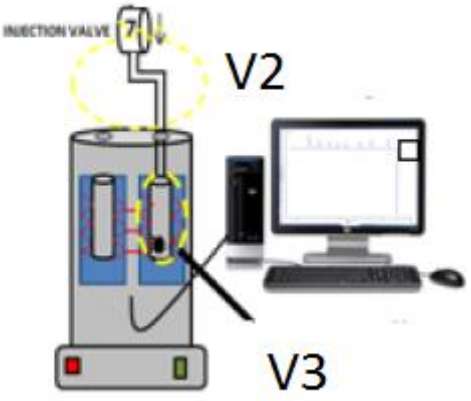

Source: Author

Since the experiment already starts in the sample cell, and the relevant dynamic variables, such as the pressure, are continuously measured, it is not necessary to model the dosing vessel and the transfer line, simplifying the model to the following equations.

$$\frac{dC_3}{dt}V_3 = -n_{outd} - m_s\frac{d\overline{q}}{dt} \tag{3.76}$$

$$P_3 = C_3 R_g T_3 \tag{3.77}$$

$$C_3 c_v \frac{dT_3}{dt}V_3 + m_s c_{ps}\frac{dT_3}{dt} + m_s c_v \bar{q}\frac{dT_3}{dt} = \frac{d}{dt}\left(\frac{P_3}{T_3}\right)T_3 V_3 + h_3 A_3(T_{cw} - T_3) + m_s\frac{d\overline{q}}{dt}(-\Delta H_{ads}) \tag{3.78}$$

In the presented case, the adjusted pressure is the cell pressure itself, described by Equation 3.79 in the same exponential function of Equation 3.41

$$P_3(t) = P_E + (P_3^I - P_E)e^{\alpha_2 t} \tag{3.79}$$

The model for the conduction in the cell wall is the same as described before as well as the boundary and initial conditions.

3.3.5 Obtaining mass transfer coefficients through optimization of the model parameters

To calculate the kinetic parameters of adsorption through the model, it is necessary to calculate, estimate or measure every experimental constants and physical properties until there is only one the mass transfer constant left for determination which is filled by either the linear driving force coefficient, k_{LDF}, or the diffusional time constant, $\frac{D_c}{r_c^2}$. The necessity of this is that these constants exhibit a large correlation with other parameters, especially h_3 , leading to multiple solutions for many initial points. However in some specific cases, both parameters can be estimated simultaneously. The calculation of the parameters is done through optimization by least squares method using the parameter estimation function of the softwares gPROMS (*Process Enterprises*, United Kingdom).

The target variable for the optimization is the heat rate detected by the microcalorimeter, as the microcalorimetric peak, the variable for the heat transfer rate is defined by Equation 3.80 and the mass transfer parameters are changed until the model transfer rate matches the experimental one, Figure 3.15. When the objective function reaches a minimum, the value of the kinetic constant is reported. The process is repeated for each peak so it works as if many diffusional experiments were done.

$$\dot{Q} = -k_{cw} A_{cw} \frac{\partial T_{cw}}{\partial r_{cw}} (r_{cw} = R_{cw0}, t) \tag{3.80}$$

Figure 3.15 – Fitting model calorimetric peak into the experimental one

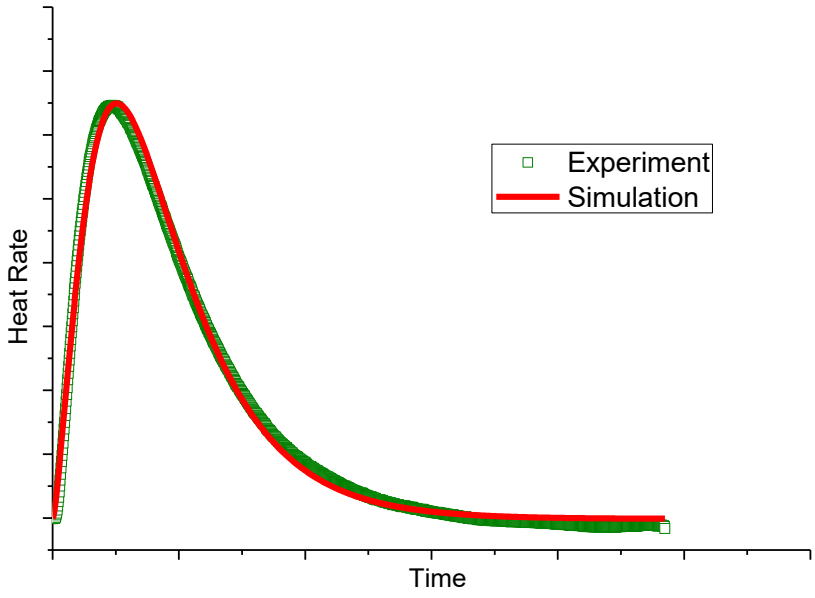

Source: Author

3.3.6 Estimating system-specific heat transfer coefficients through blank experiments

The dynamic model introduces the initially undetermined heat transfer coefficients, namely h_1A_1, h_2A_2, h_3 and K. In the same way as the volume of the domains, the coefficients can be estimated through blank experiments, either in the adsorption method or the desorption method. The process for calculating is the same as the one for the mass transfer coefficients, but since there is no adsorption, the degrees of freedom of the system are on the heat transfer parameters and the optimization is done so that the modeled calometric peak on the blank

experiment matches the experimental one. The dynamic energy balance equations for the blank experiments are explicit below. Equations 3.81, 3.82, 3.83 and 3.84.

$$C_1 c_v \frac{dT_1}{dt} V_1 = \frac{d}{dt}\left(\frac{P_1}{T_1}\right) T_1 V_1 + h_1 A_1 (T_{o1} - T_1) \tag{3.81}$$

$$C_2 c_v \frac{dT_2}{dt} V_2 = \dot{n}_{out} c_v (T_1 - T_2) + \frac{d}{dt}\left(\frac{P_2}{T_2}\right) T_2 V_2 + h_2 A_2 (T_{o1} - T_2) \tag{3.82}$$

$$C_3 c_v \frac{dT_3}{dt} V_3 + m_s c_{ps} \frac{dT_3}{dt} = \frac{d}{dt}\left(\frac{P_3}{T_3}\right) T_3 V_3 + h_3 A_3 (T_{cw} - T_3) \tag{3.83}$$

$$-k_{cw} A_{cw} \frac{\partial T_{cw}}{\partial r_{cw}} (r_{cw} = R_{cw0}, t) = -K(T_{o2} - T_{cw}) \tag{3.84}$$

With all parameters defined, the mass transfer coefficients can be calculated and the results discussed.

3.4 Parameter values and isotherm models used

Table 3.1 contains the general used constants, physical properties and dimensions used in the model.

Table 3.1 – Global parameters and physical constants

Parameter values	
Calorimeter temperature (T_{o2})	298.15 K
Ambient temperature (T_{o1})	294.15 K
Pressure Range	From vacuum to 1.2 bar
A_3	0.00305 m²
A_{cw0}	0.00386 m²
c_p	37.6 J/(mol.K)
c_{cw}	502 J/(kg.K)
c_{ps}(NoritRB4)	711 J/(kg.K)
c_{ps}(Zeolite 13X)	915 J/(kg.K)

Table 3.1 – Global parameters and physical constants (contd.)

Parameter values	
c_{ps}(Zeolite NaZsm5)	915 J/(kg.K)
h_1A_1	1.12 W/K
h_2A_2	0.01 W/K
K	3.00 W/K
k_{cw}	15 W/(m.K)
m_s (NoritRB4)	1.34E-4 kg
m_s(Zeolite 13X)	7.73E-5 kg
m_s(Zeolite NaZsm5)	1.79E-4 kg
R_{cw}	0.00587 m
R_{cw0}	0.00743 m
R_{cal}	0.0560 m
ρ_{cw}	7850 kg/m³
V_1	15.4E-6 m³

Source: Author

The isotherm model used for all adsorbents was Sips model (Sips, 1948). Equation 3.85

$$q_E = \frac{\overline{q}_m b P^n}{1 + bP^n} \tag{3.85}$$

4 RESULTS AND DISCUSSION

This section presents the relevant results of many experiments done to estimate the kinetic parameters through the derived models. Interpretation of the results, comparison of obtained data with published literature, discussion on difficulties and inaccuracies and refinements are also presented and discussed.

4.1 Phenomenological analysis of the response curve

This type of analysis helps to understand the physical aspects of the response heat rate curve from the experiments. In order to make a correct measure of diffusion, it is necessary to properly evaluate the influence of all mass and heat transfer resistances of the systems. Once a proper understanding of the microcalorimetric peak is established, limits of the model can be pointed and evaluation of errors are facilitated. The phenomenological analysis was done using the reviews of the piezometric methods by Brandani (1998), Grenier(1994) and Grenier (1995).

4.1.1 Response of Blank Experiments

Recalling Equation 3.78 as Equation 4.1, energy accumulation in the system is the sum of temperature change induced by change of pressure plus the heat transfer to the ambient. In adsorption experiments, the pressure change is positive and for desorption, negative, and the heat transfer is the opposite in each scenario. In order to have a more straightforward analysis, the desorption method model will be used for the discussion.

$$C_3 c_v \frac{dT_3}{dt} V_3 + m_s c_{ps} \frac{dT_3}{dt} = \frac{d}{dt}\left(\frac{P_3}{T_3}\right) T_3 V_3 + h_3 A_3 (T_{cw} - T_3) \tag{4.1}$$

Experimentally, it is verified that the conduction heat transfer resistance is negligible, thus the dominant resistance is of convection. Since the response curve measures the heat rate through the cell walls, the response curve is equal to the heat transferred through convection, Equation 4.2.

$$\dot{Q} = h_3 A_3 (T_3 - T_{cw}) \tag{4.2}$$

Assuming initially that the heat transfer coefficient h_3 is independent of pressure, variable T_3 will control the form of the curve, as the temperature of the cell wall remains essentially constant. The temperature decrease is controlled by the rate of pressure decrease, $\frac{dP_3}{dt}$, which is determined by parameter α_2 from Equation 3.80, which is essentially the valve

restriction to flow. At a given heat transfer coefficient, the effect of the valve restriction is illustrated in Figure 4.1

Figure 4.1 – Effect of valve restriction in response curve

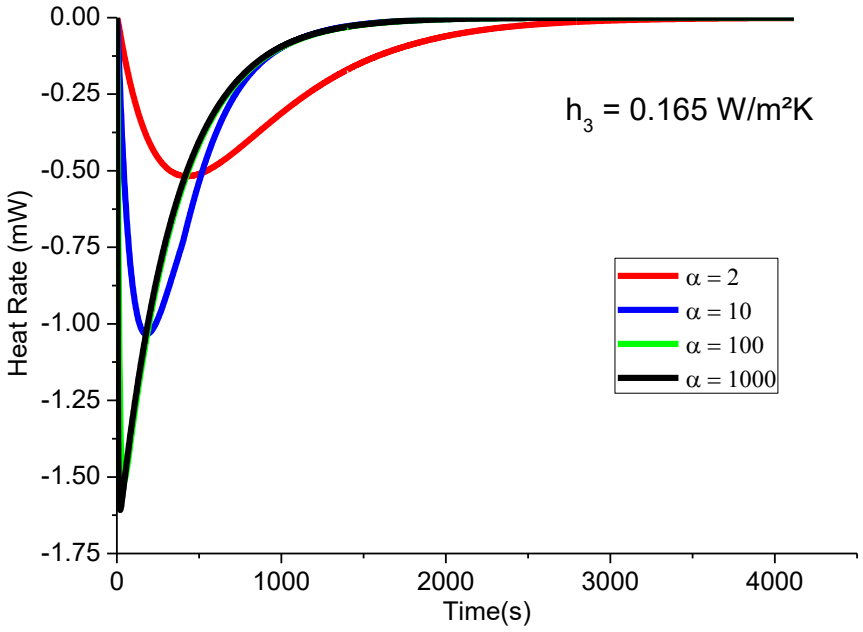

Source: Author

Figure 4.1 shows that the effect of the pressure change velocity has an upper limit, if the valve restriction is low enough so that the pressure decreases in a step-like profile. The temperature change is almost instantaneous and the microcalorimetric peak reaches a maximum value in a very short time, the heat transfer rate is controlled by pressure change at this stage. After the limit is reached, the return to the baseline is controlled by convection, as seen by the constant behavior of the curve for $\alpha_2 = 100$ and 1000.

If, however, the valve restriction is large, pressure change and convection will control the heat rate curve at all times. Experimentally these results indicate that for the evaluation h_3 the better scenario is that of a step pressure change in the domain, eliminating the pressure effect after the peak reaches a maximum. However, it is also possible to estimate the coefficient in a situation of large valve restrictions, but the pressure measurements need to be precise, due to the high sensibility of the parameters to the model.

4.1.2 Response of desorption experiments

The main concern at measuring diffusivities experimentally is to prevent that the diffusional process is too fast compared to other mass or heat transfer processes, if the diffusional resistances become negligible, no useful results can be extracted from experimental data. Recalling Equation 3.63 as Equation 4.3, the response curve will depend on three resistances: Flow restrictions due to the valve, convective heat transfer resistance and diffusional mass transfer resistance.

$$C_3 c_v \frac{dT_3}{dt} V_3 + m_s c_{ps} \frac{dT_3}{dt} + m_s c_v \bar{q} \frac{dT_3}{dt} = \frac{dP_3}{dt} V_3 + h_3 A_3 (T_{cw} - T_3) + m_s \frac{d\bar{q}}{dt} (-\Delta H_{ads}) \quad (4.3)$$

Valve restrictions can be controlled experimentally, so the flow restriction limitations are, in theory, possible to reduce or eliminate. The first scenario to analyze is one of low flow restrictions for different velocities of diffusion, Figure 4.2. Theoretically, this set up would be the best to measure a more wide range of diffusional time constants, due to fewer resistances.

Figure 4.2 – Sensibility of the response curve to different diffusional time constants at low valve restrictions

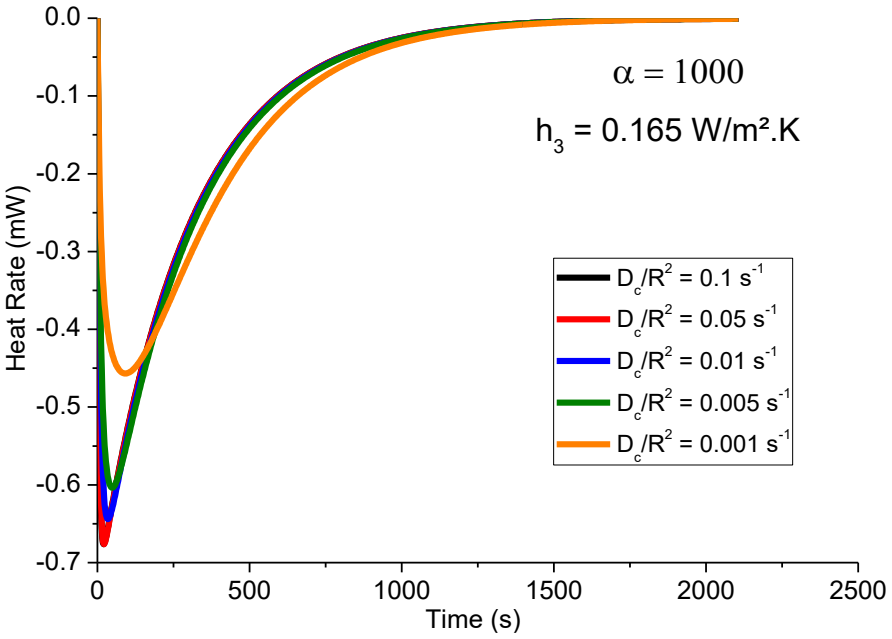

Source: Author

Apparently significant effect on the curve arises at $\frac{D_c}{r_c^2} = 0.005\ s^{-1}$, but by changing the plot scale to shorter times, a larger sensibility is unraveled, Figure 4.3. It is important to note that the area of the curve corresponding to the return to the baseline has a constant behavior for $\frac{D_c}{r_c^2} > 0.001\ s^{-1}$ which indicates that the convective resistance controls the heat transfer at these times.

Figure 4.3 – Short time sensibility of the response curve to different diffusional time constants at low valve restrictions

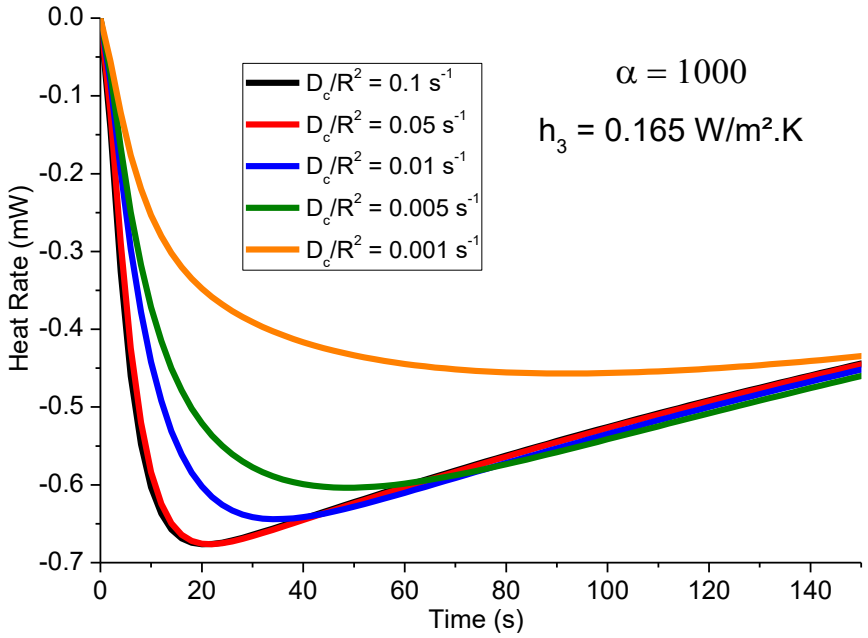

Source: Author

The previous figure shows that the actual sensitivity for this setup begins at $\frac{D_c}{r_c^2} = 0.01\ s^{-1}$. This result is consistent with the results of Grenier *et al*. (1995), which the authors conclude that diffusion controls the initial increase of temperature that is reflected in the calorimeter by the initial rise in the heat rate. Another important consequence of this behavior is that it is not necessary to fit the model to the entire peak, if adsorption is fast enough so that heat transfer resistances dominate the stabilization of the curve. Moreover, the convective control at long times for fast diffusing species indicates that the heat transfer coefficient can be obtained without the use of blank experiments, by fitting the later times of the curve.

A second scenario for the measurement of a moderate valve restriction, looking at the short time behavior of Figure 4.4, sensibility is lost, reliable results arise for values of $\frac{D_c}{r_c^2} = 0.005\ s^{-1}$ and lower. This is consistent with the relative importance of the mass transfer

resistances, a more restricted valve will rise flow resistance, making it more relevant in relation to diffusional resistance.

Figure 4.4 – Short time sensibility of the response curve to different diffusional time constants at moderate valve restrictions

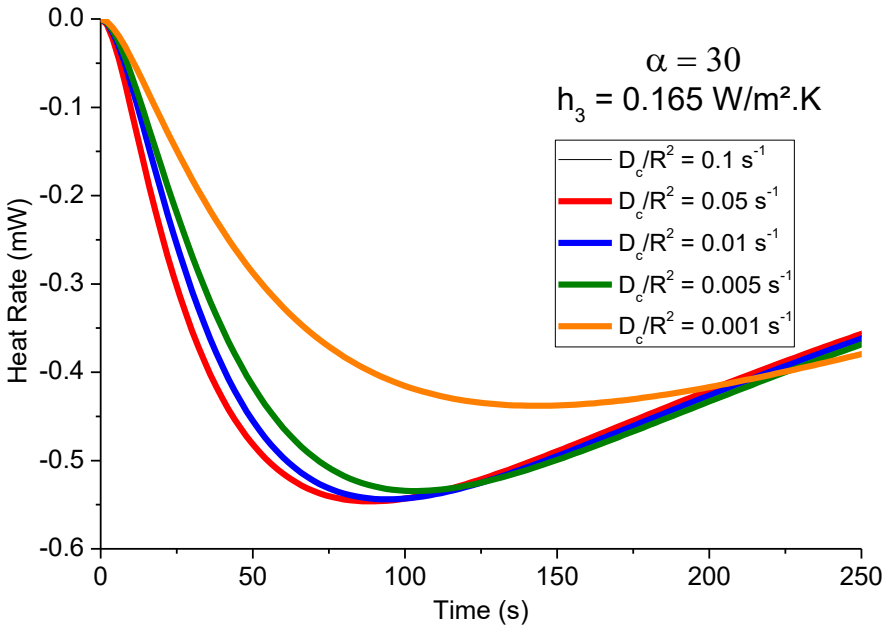

Source: Author

Lastly, the third scenario consists in a highly restricted valve, Figure 4.5. A very significant drop in the model resolution is obtained, considering experimental variations, only diffusional time constants at the vicinity of $0.001\ s^{-1}$ and lower could be measured. Again, this result is consistent as it shows that the flow restriction is too large that it dominates the mass transfer.

Figure 4.5 – Short time sensibility of the response curve to different diffusional time constants at large valve restrictions

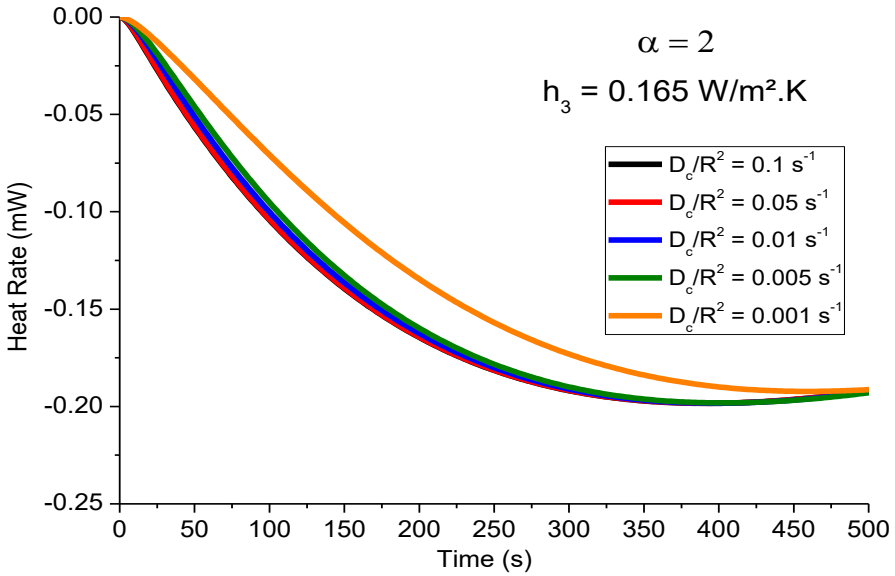

Source: Author

Another relevant effect is of the convective heat transfer coefficient itself. In theory its not possible to control this value experimentally, but at a given value the influence of the convective heat transfer resistance may be significant or not, and if the value is within a range where it does not control the response curve, the parameter would not need to be estimated. Figure 4.6 and Figure 4.7 shows that h_3 impacts the curve at any time, that is, it's not possible to isolate a section of the response curve where the convective heat transfer effect is negligible, although the parameter has an upper limit where further increase in it will not influence the heat rate. However, considering that the main convection mechanism in the experiment is natural convection, it is unlikely that the value of h_3 could reach such high values.

Figure 4.6 – Sensibility of the response curve to different heat transfer coefficients at low valve restrictions

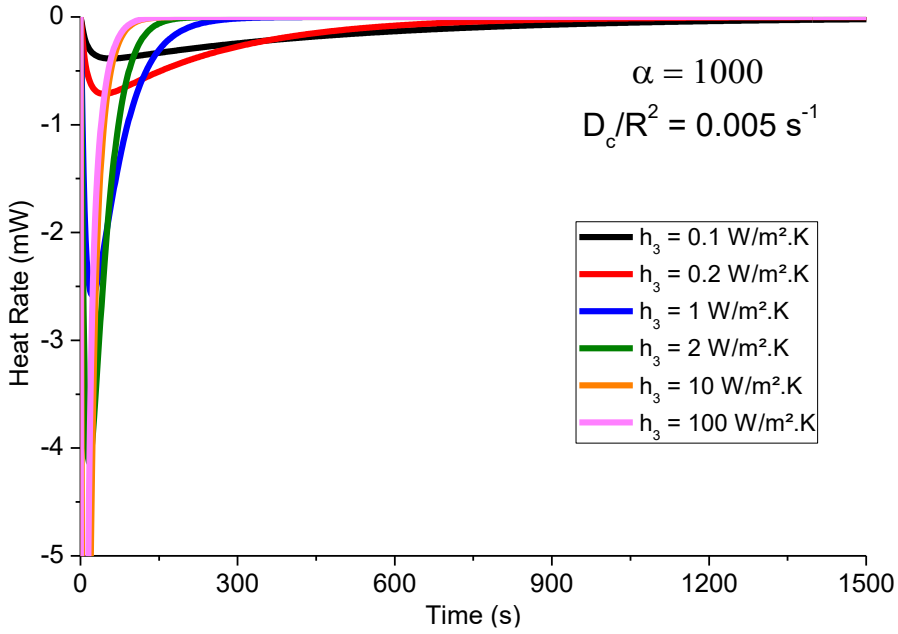

Source: Author

Figure 4.7 – Short Time sensibility of the response curve to different heat transfer coefficients at low valve restrictions

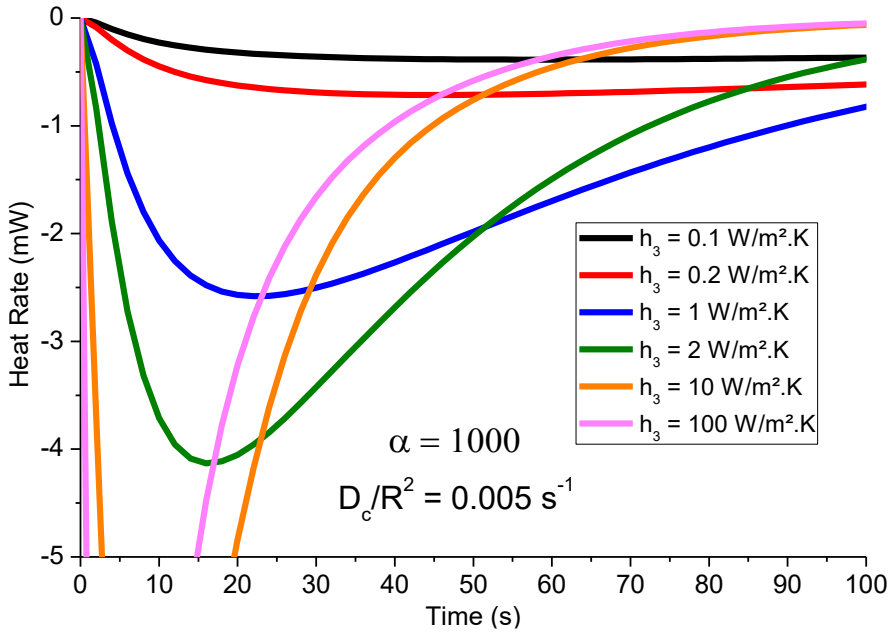

Source: Author

The effect of the heat transfer parameter on the model shows that it is necessary a precise and reliable measure of it as the model has a very high sensibility to it. Moreover, as Figure 4.1 shows, in fast diffusing systems, convective resistances dominate the stabilization of the curve,

so h_3 can be calculated by fitting the second half of the peak by neglecting the diffusional time constant value.

4.2 Fine-tuning of the heat transfer coefficients measurement.

The impact of the convection heat transfer was demonstrated by the previous analysis, which prompts a reliable method for measuring coefficient h_3. Adsorption method also has two more constants, h_2 and h_1 but initial tests with the model discarded any significant influence of those two parameters, thus they were fixed with the areas A_1 and A_2 as a global constant, which was previously shown in Table 3.1. Figures 4.8 and 4.9 show the overall no impact of those parameters on the model.

Figure 4.8 – Tests of the impact of constant h_1A_1 into the model

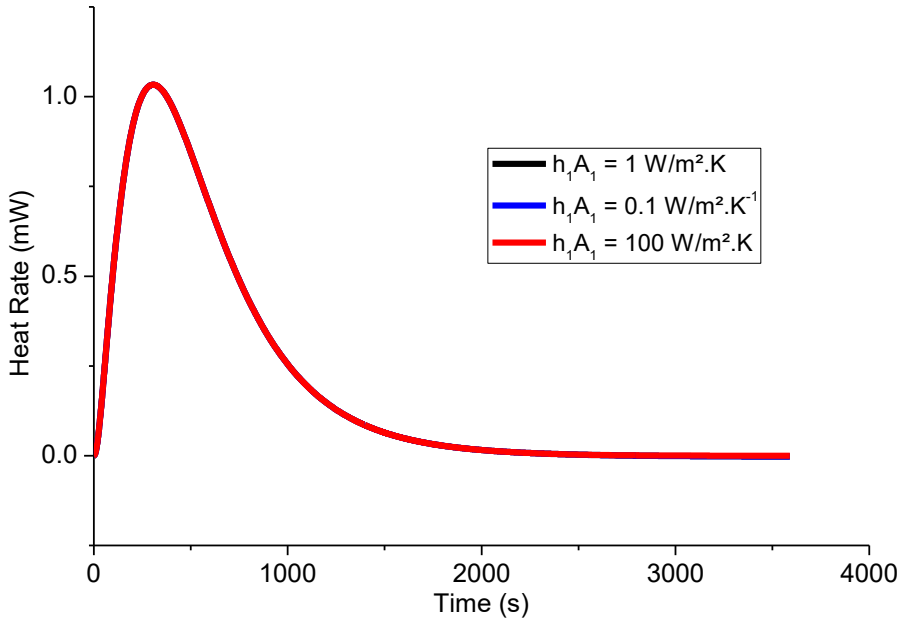

Source: Author

Figure 4.9 – Tests of the impact of constant h_2A_2 into the model

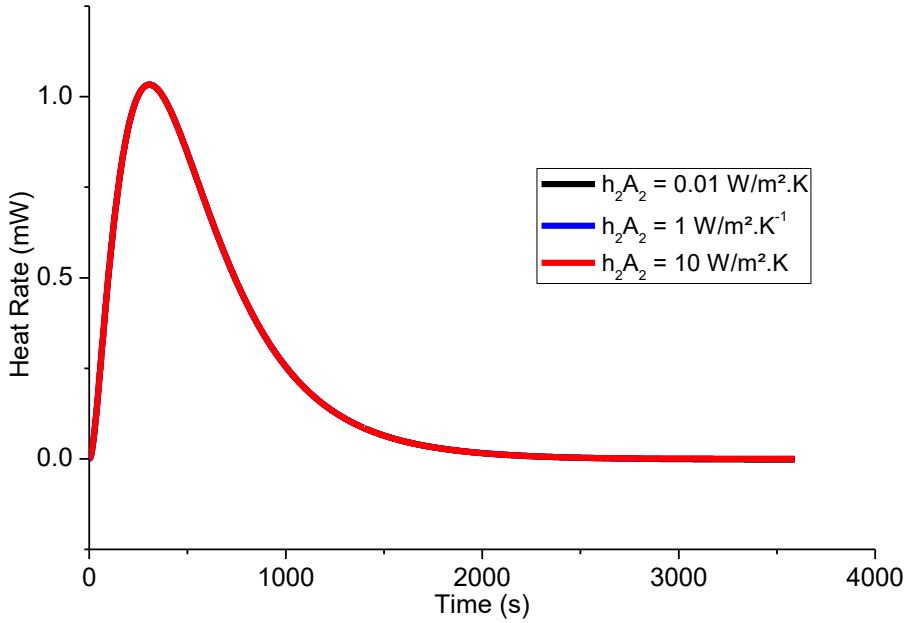

Source: Author

For simplicity yet again, the model used for the measurement of h_3 was the desorption one. It was previously explained that it is possible to calculate this parameter through the blank experiments. An initial assumption in the previous section was that the coefficient would be independent of the valve restriction at the experiment, this hypothesis was tested in different blank runs and the results point that there is no apparent significance of parameter α_2 on the value of the convection heat transfer parameter, as seen in following Figures 4.10, 4.11 and 4.12.

Figure 4.10 – Measured value of h_3 in blank experiments with low valve restriction

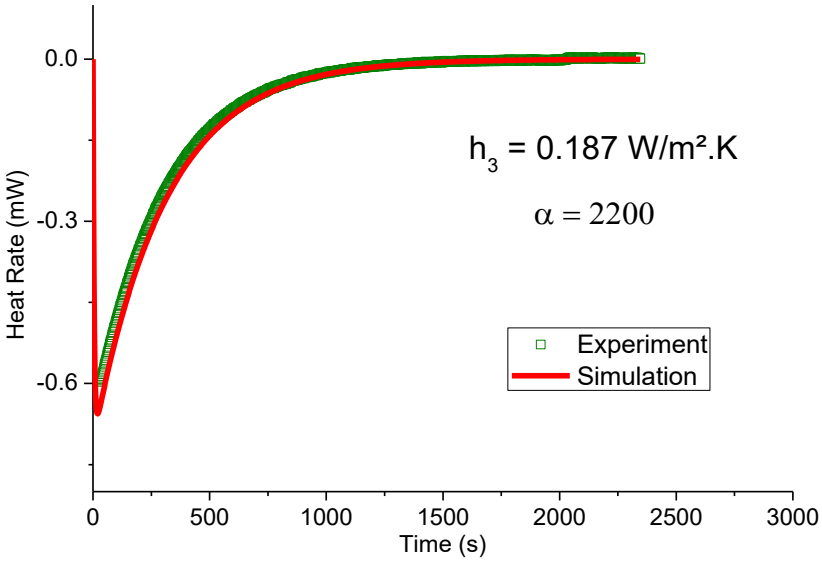

Source: Author

Figure 4.11 – Measured value of h_3 in blank experiments with moderate valve restriction

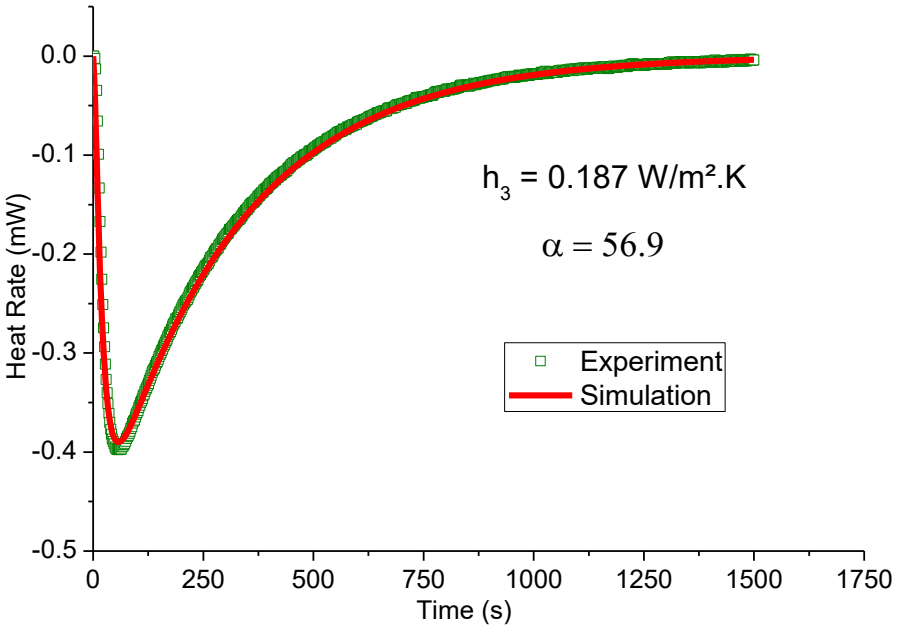

Source: Author

Figure 4.12 – Measured value of h_3 in blank experiments with large valve restriction

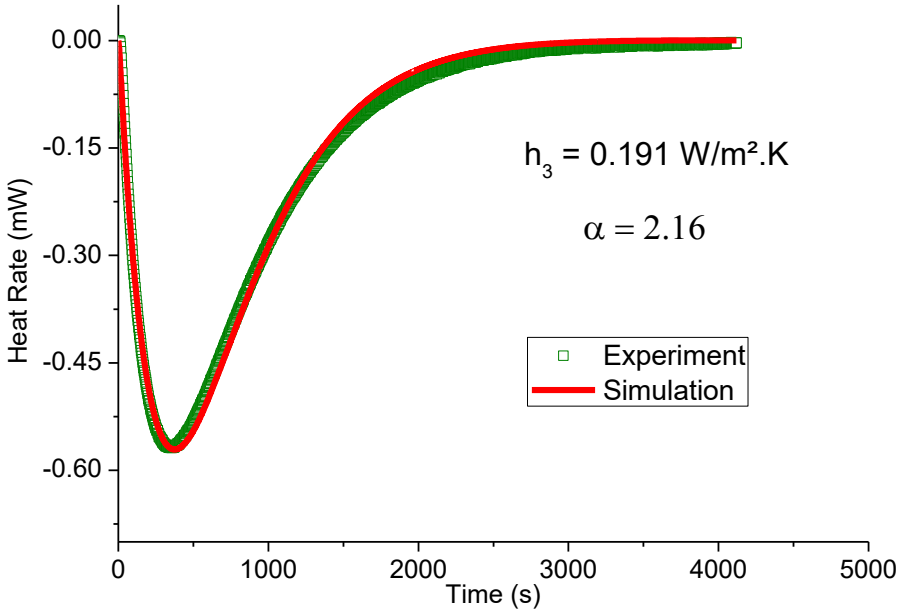

Source: Author

Although the results are reasonably consistent with a single value that is independent of α_2, the results presented are for the same sample of sorbent, Zeolite NaZSM-5 for different samples this result is less consistent. Figure 4.13 shows the adjusted parameter for sample of activated carbon NoritRB4, and there is a significant difference between the samples.

Figure 4.13 – Measured value of h_3 for NoritRB4

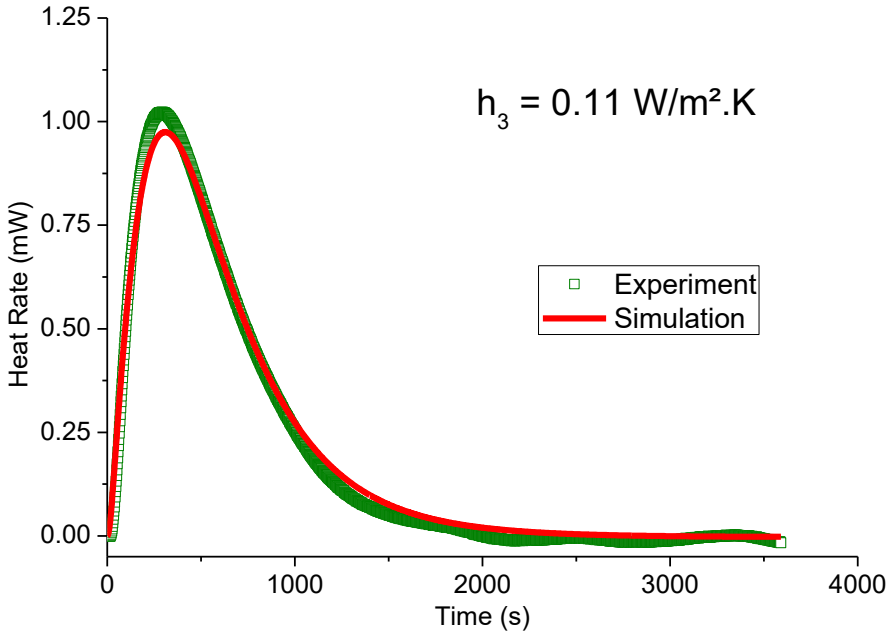

Source: Author

Therefore, it should be assumed that each sorbent will have a different value of h_3, so for each sample of sorbent it will be necessary to perform both the sorption experiments and the blank experiments, so that the diffusion parameters calculated are reliable. A hypothesis for the different values is that the coefficient will depend on particle radius. Zeolite sample is in form of powder and the activated carbon is in form of pellets, so effects of fluid stagnation could play a part in these results.

It should be remembered that, as seen in the previous section, the blank experiments are not necessary to calculate the heat coefficient for fast-diffusion species, therefore, for better control of the results, if the sample shows a fast enough diffusion properties, adjusting the thermal stabilization of the curve in a regular experiment to obtain the value of h_3 is preferable. However, for a more global way of measurement, the blank experiments cover all types of solids.

4.3 Preliminary results using the adsorption method.

The first tested sample of adsorbent was one of commercial activated carbon Norit RB4, the mass transfer model used was Linear Driving Force, as activated carbons have a wide range

of pore size distributions, so it is expected that multiple diffusional resistances take part in the process. The sorbate used was carbon dioxide, CO_2. Table 4.1 contains the Sips Isotherm parameters for CO_2 – Norit RB4, Figure 4.14 the isotherm fitting and Figure 4.15 shows the differential Enthalpy curve for the system, all data was calculated experimentally on the calorimeter.

Table 4.1 – Isotherm parameters adjusted for CO_2 – NoritRB4

Sips Isotherm Parameters	
qm (mmol/g)	2.93
b (Pa^{-1})	8.32E-6
n	1.02

Source: Author

Figure 4.14 – Sips Isotherm Fitting for CO_2 – NoritRB4 system

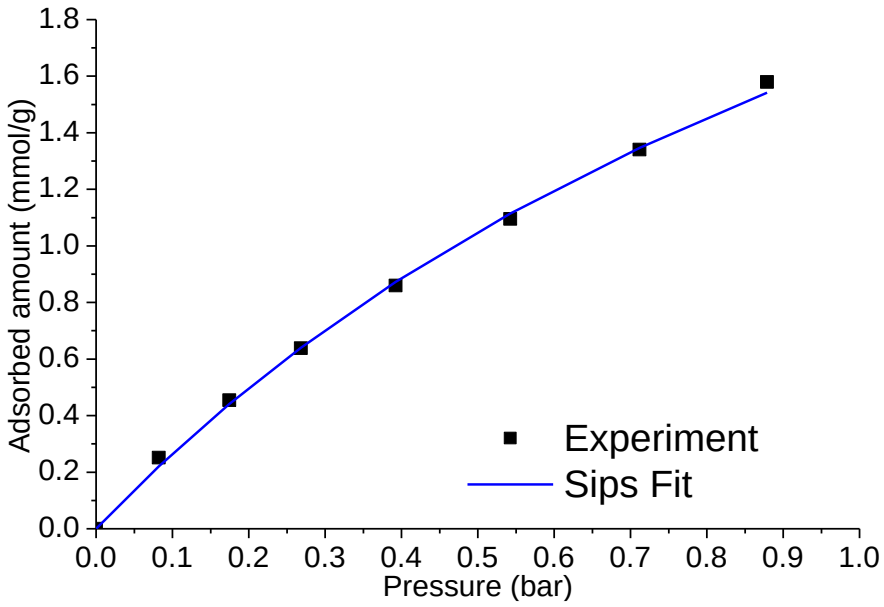

Source: Author

Figure 4.15 – Differential Enthalpy Curve for CO_2 – NoritRB4 system

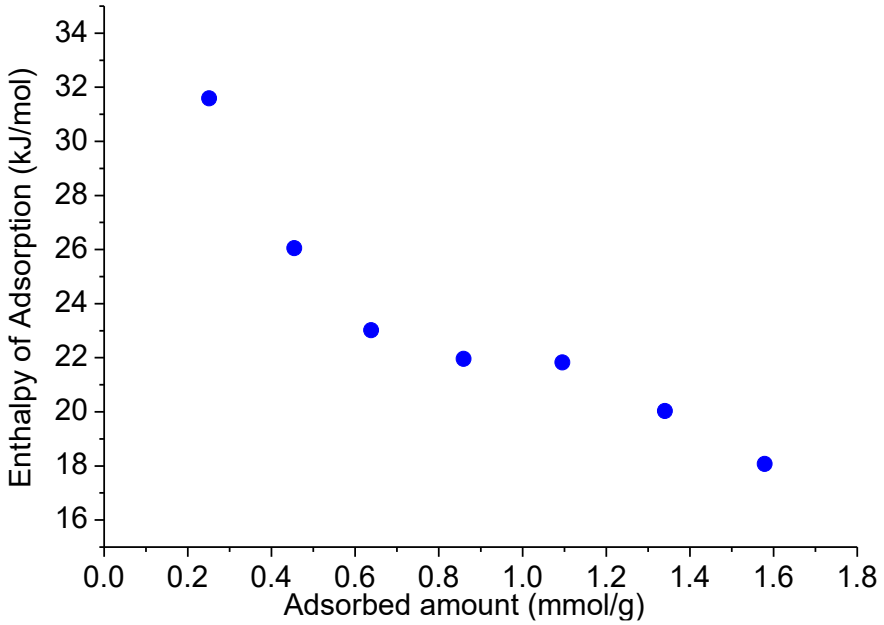

Source: Author

Figures 4.16, 4.17 and 4.18 show the results of the fittings by using the model simulations. Model adjustment to experimental data was satisfactory. The optimized value for K_{LDF} is within the range reported by literature at Siqueira et.al (2018) at value of 0.1 s^{-1}, the comparison of global coefficients can be done because the tested sample in this work is the same sample used in the referenced paper. The heat transfer coefficient was calculated by simultaneous fitting with K_{LDF} , the value for all peaks were approximately equal, then all of them were reduced to the same value that was applied to all the curves again, resulting in the final value for the kinetic constant.

Figure 4.16 – Result of the fitting of the model to experimental results. CO_2 – NoritRB4. Dosing Vessel Initial Pressure: 43556 Pa. Cell Initial pressure: 17470 Pa. Equilibrium Pressure: 26834 Pa

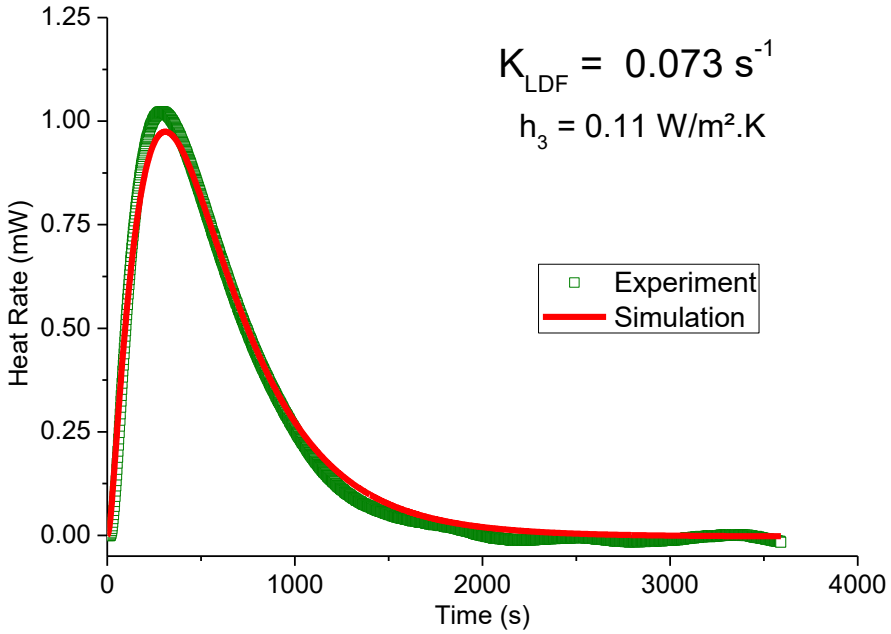

Source: Author

Figure 4.17 – Result of the fitting of the model to experimental results. CO_2 – NoritRB4. Dosing Vessel Initial Pressure: 60979 Pa. Cell Initial pressure: 26834 Pa. Equilibrium Pressure: 39250 Pa

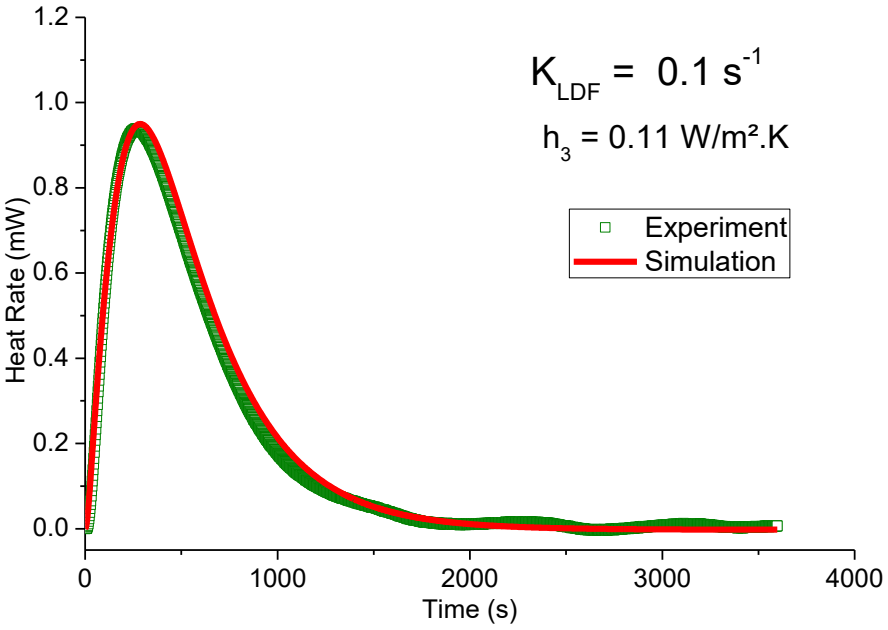

Source: Author

Figure 4.18 – Result of the fitting of the model to experimental results. CO_2 – NoritRB4. Dosing Vessel Initial Pressure: 79886 Pa. Cell Initial pressure: 39250 Pa. Equilibrium Pressure: 54225 Pa

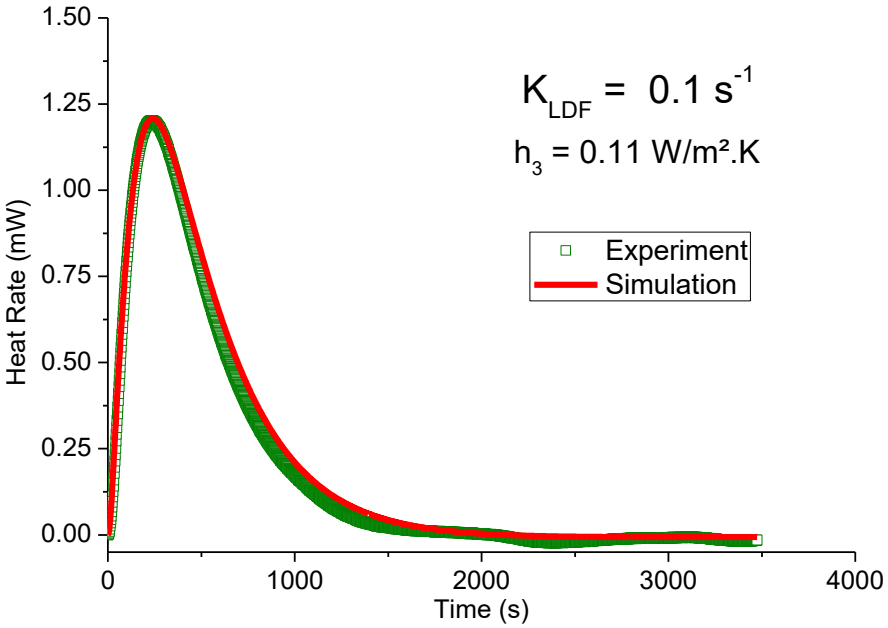

Source: Author

Although the algorithm optimization only yields a single result, a sensitivity analysis is necessary due to the possibility of a too fast diffusion that is in the bounds of the method to be measured. Figure 4.19 shows the short time sensitivity of the curve at different linear driving force constants. The sensibility of the model at these values of K_{LDF} is already low, meaning that intraparticle diffusion is too fast to be properly measured, a more accurate result would be to establish an inferior limit to the value of the constant, so the actual calculated value is at the range of $K_{LDF} = 0.05\ s^{-1}$ and beyond. A clearer way of evaluating the sensitivity is to compute de average deviations from the simulated results with the experimental data, as Figure 4.20 shows. All tested results have an average deviation inferior to 5% , and for every value above $K_{LDF} = 0.2\ s^{-1}$ the deviations are equal, showing insufficient experimental conditions for the measurement.

Figure 4.19 – Short time sensitivity of the model at different K_{LDF}. CO_2 – NoritRB4 system. Dosing Vessel Initial Pressure: 43556 Pa. Cell Initial pressure: 17470 Pa. Equilibrium Pressure: 26834 Pa

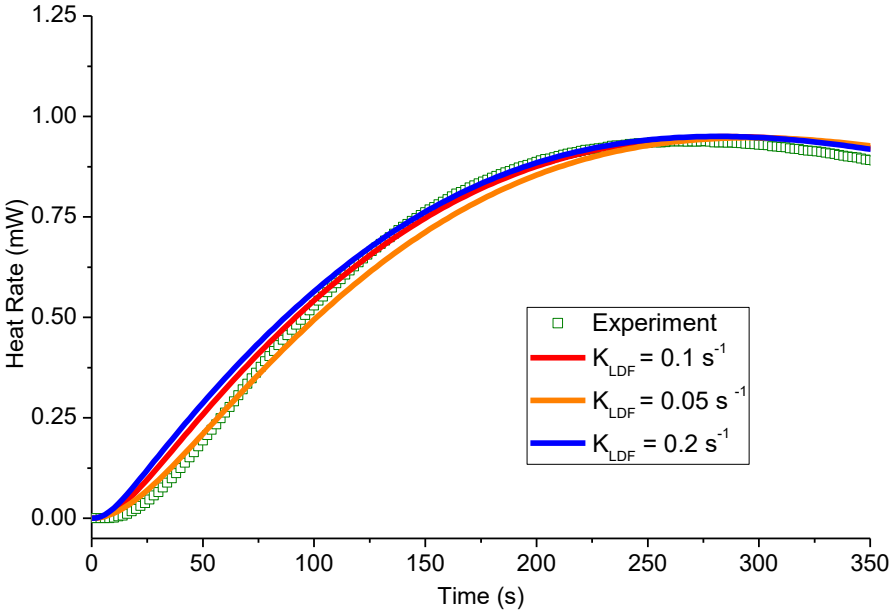

Figure 4.20 – Short time sensitivity of the model at different K_{LDF}. Average Deviations from experimental data.

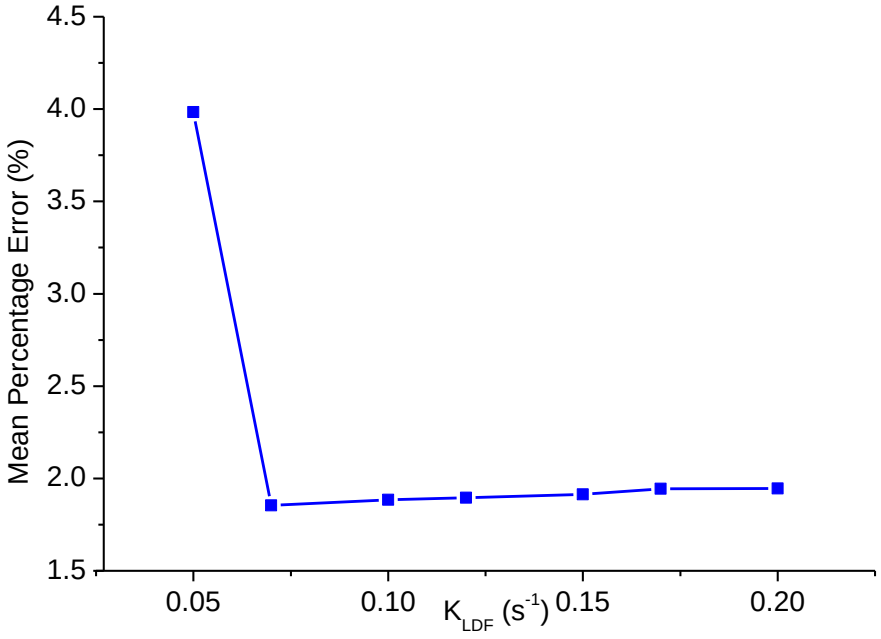

A second tested sorbent was of commercial pellets of Zeolite 13X with the same CO_2 sorbate. With the pelletized version of the sorbent, it is expected that macropore effects take

place in the mass transfer process, but a weak assumption is done by assuming that intracrystalline diffusion controls the process, so the intraparticle diffusional control model was used, assuming an effective diffusion coefficient as the result . Table 4.2 shows the isotherm parameters for Zeolite 13X – CO_2, Figure 4.21 contains the fitting and Figure 4.22 shows the differential enthalpy curve.

Table 4.2 – Isotherm parameters adjusted for CO_2 – Zeolite 13X

Sips Isotherm Parameters	
qm (mmol/g)	6.55
b (Pa^{-1})	0.0149
n	0.435

Source: Author

Figure 4.21 – Sips Isotherm Fitting for CO_2 –Zeolite 13X system.

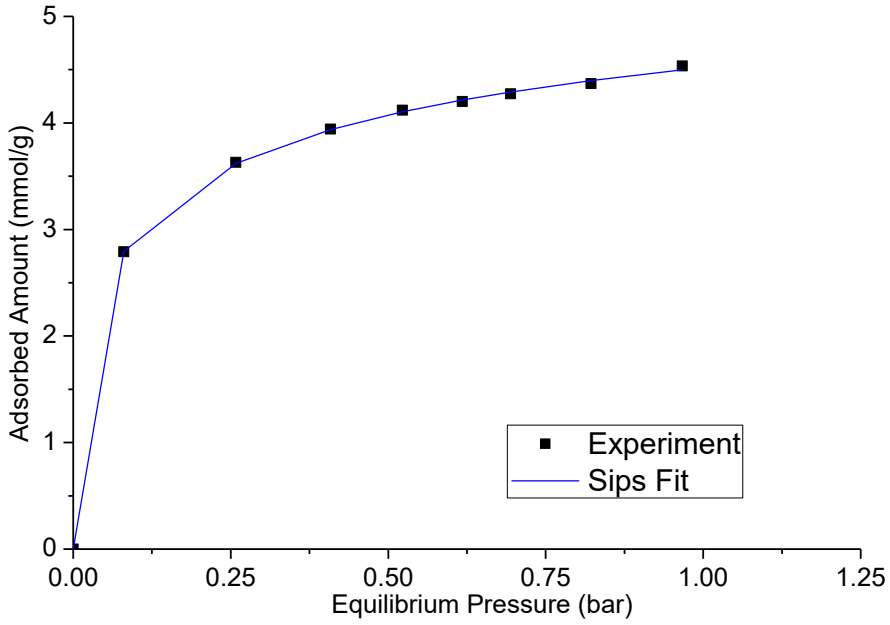

Source: Author

Figure 4.22 – Differential Enthalpy Curve for CO_2 – Zeolite 13X system.

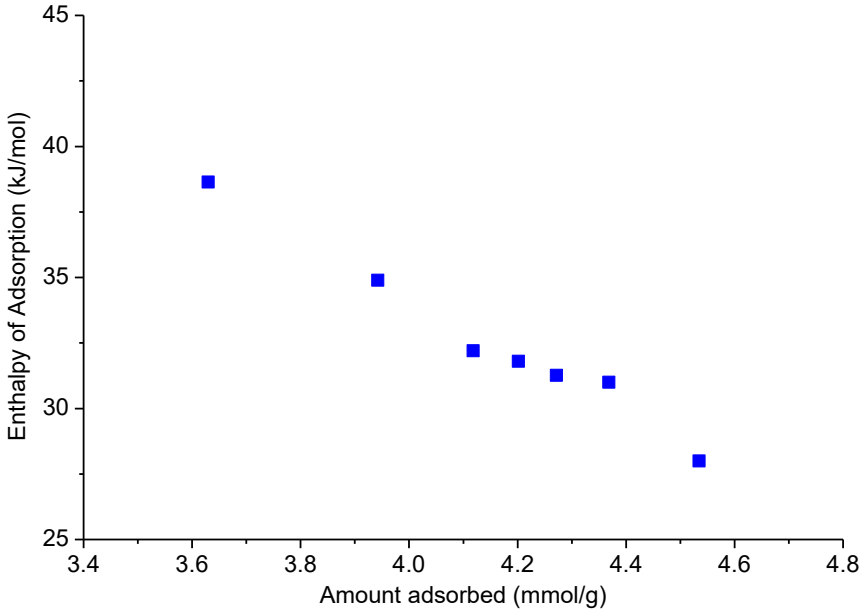

Source: Author

Figures 4.23, 4.24 and 4.25 show the results of the optimization of the diffusional time constant to fit the experimental data. The simulation was adjusted well to the experimental data, and the values for $\frac{D_{eff}}{r_c^2}$ exhibit little variation. However, for an accurate interpretation of the results, it is important to note that the presented results are in very different pressure conditions, considering the previous mentioned isotherm.

Figure 4.23 – Result of the fitting of the model to experimental results. CO_2 – Zeolite13X. Dosing Vessel Initial Pressure: 58484 Pa. Cell Initial pressure: 8052 Pa. Equilibrium Pressure: 25822 Pa.

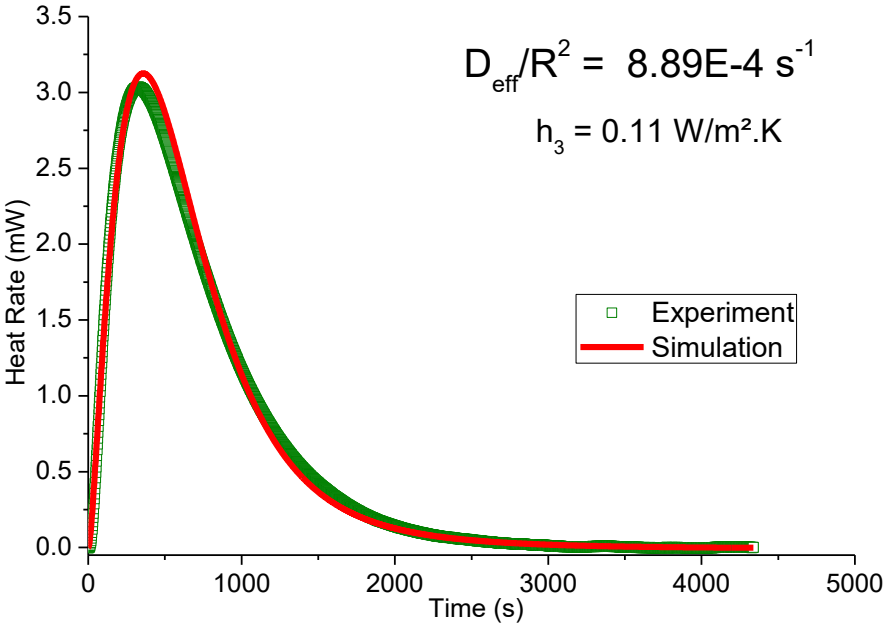

Source: Author

Figure 4.24 – Result of the fitting of the model to experimental results. CO_2 – Zeolite13X. Dosing Vessel Initial Pressure: 116892 Pa. Cell Initial pressure: 82191 Pa. Equilibrium Pressure: 96662 Pa.

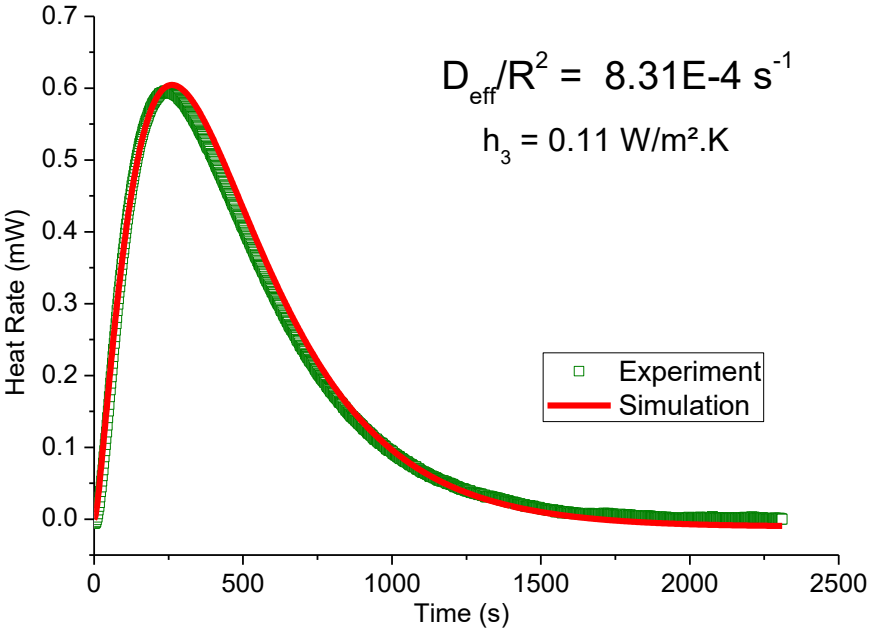

Source: Author

Figure 4.25 – Result of the fitting of the model to experimental results. CO_2 – Zeolite13X. Dosing Vessel Initial Pressure: 115942 Pa. Cell Initial pressure: 71189 Pa. Equilibrium Pressure: 87885 Pa.

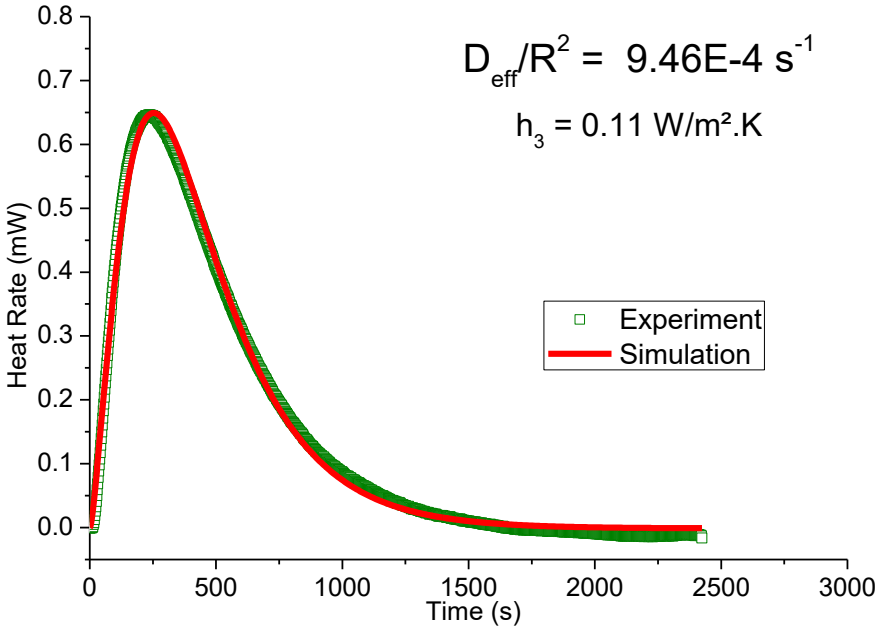

Source: Author

Contrary to the isotherm of NoritRB4, which has a linear behavior in the observed range, the isotherm of the zeolite is non-linear; this profile should cause changes in the measured diffusivities due to the thermodynamic effect that is corrected by Darken's factor. Figure 4.26 shows a graph that correlates the logarithm of the pressure with the logarithm of the amount adsorbed. Taking the derivative of the function, it is obtained the expected values of the diffusivities, assuming that the first point of the isotherm, which corresponds to the peak of Figure 4.16, is within the limits of Henry Law. Table 4.3 contains the expected values for the constants.

Figure 4.26 – Correlating the logarithms of pressure and amount adsorbed to correct measured diffusivities

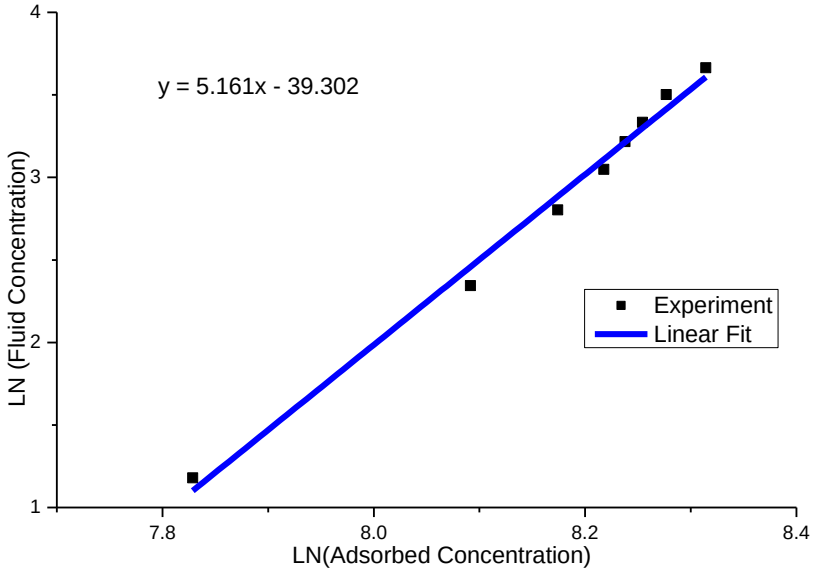

Source: Author

Table 4.3 – Comparison between calculated and expected corrected diffusivities

Corrected Diffusional Time constants		
	Calculated Value	Corrected value
Figure 4.16	8.89E-4 s^{-1}	8.89E-4 s^{-1}
Figure 4.17	8.31E-4 s^{-1}	1.48E-4 s^{-1}
Figure 4.18	9.46E-4 s^{-1}	1.68E-4 s^{-1}

Source: Author

Even if the lowest point of the isotherm is not on the limits of Henry law, it is clear from the profile that the diffusivities at these three conditions must be different. Therefore, the results are not where they were expected to be, which may be explained by macropore influences that would reduce effective diffusivity, experimental inadequacies or errors in the calculation of the heat transfer coefficient.

A reference for the diffusional time constant calculation of the analyzed system is found in Silva *et al*. (2012). Care must be taken when comparing the results, as both samples are pelletized and the crystalline average radius could be different from one sample to other, therefore, direct comparison of the results are not rigorously accurate. However, most commercial zeolites have similar crystal diameter, so a rule-of-thumb value can be assumed for comparison. The mentioned paper works in the limit of Henry law, so the proper calculated value that can be used is the one from Figure 4.16.

The lowest temperature data from the previous work is at 313 K, different from 298K used in the described experiments. Nonetheless, assuming weak temperature dependence for diffusion at this range, the obtained values from the paper are at an average value of 0.00109 s^{-1} while the calculated value from the calorimeter is 8.89E-4 s^{-1}. As expected, the value for the lower temperature is also lower and both values are close in terms of order of magnitude, so a potential capability of accurate measured is shown by using the new method.

Figure 4.27 shows the short time sensitivity analysis of the response curve to different kinetic constant values. Contrary to the results for NoritRB4, the present curves show a clear sensibility to small changes in the diffusion constant, therefore the experimental conditions for the estimation are adequate and the final result for $\frac{D_{eff}}{r_c^2}$ is at the range of 8.5E-4 s^{-1} to 1E-3 s^{-1}. This result can be extracted with more precision by analyzing the average deviations from experimental data, Figure 4.28. Table 4.4 contains the statistical evaluation of the parameter.

Figure 4.27 – Short time sensitivity of the model at different D_{eff}/r_c^2. CO_2 – Zeolite 13X system. Dosing Vessel Initial Pressure: 58484 Pa. Cell Initial pressure: 8052 Pa. Equilibrium Pressure: 25822 Pa.

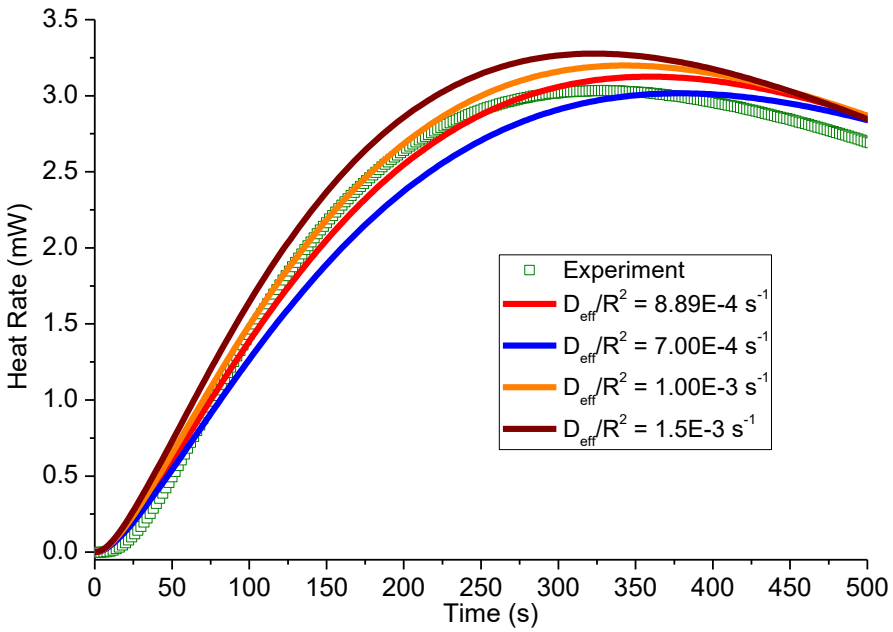

Source: Author

Figure 4.28 – Short time sensitivity of the model at different D_{eff}/r_c^2. CO_2 – Zeolite 13X system. Average Deviations from experimental data.

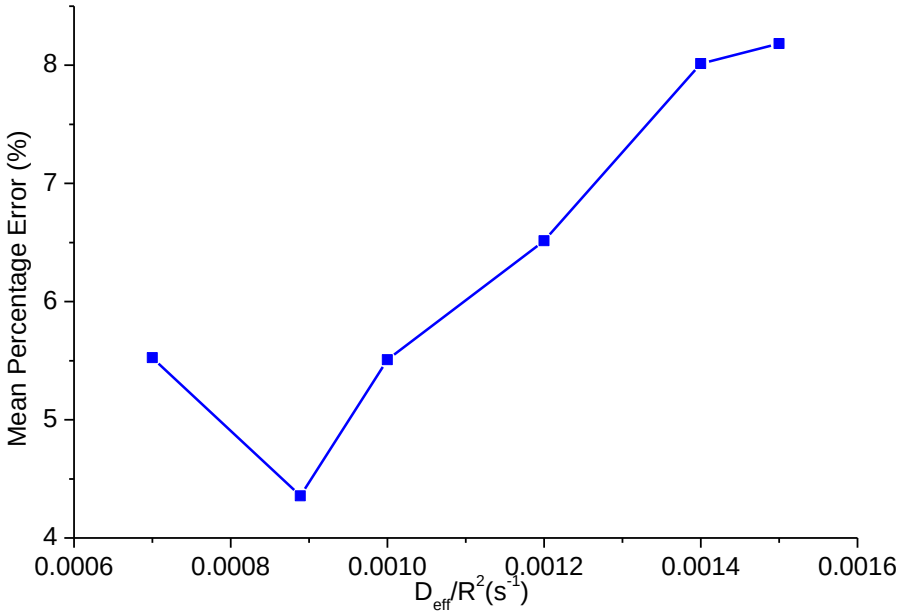

Source: Author

Finally, assuming intracrystalline diffusion as the dominant process of mass transfer, and using rule of thumb values for commercial zeolites for the crystal diameter (~ 2μm) (Silva *et al*. 2012), the diffusional time constant can be converted to actual Diffusivity, D_c , as it can be seen from Table 4.5, the calculated value is in a good agreement with published literature. Table 4.5 also summarizes the presented and discussed preliminary results, comparison with literature and adequacy for measurement.

Table 4.4 – Statistical evaluation of diffusion parameter

Statistical evaluation of $\frac{D_{eff}}{r_c^2}$ (s^{-1})			
Best Fit Value	Mean	Standard Deviation	Confidence Interval (95%)
8.89E-4 s^{-1}	8.65E-4 s^{-1}	5.91E-5	±1.16E-4

Source: Author

Table 4.5 – Summary of the preliminary results

Calculated kinetic parameters			
Adsorbent	Calorimetry	Literature	Within measurement range?
Norit RB4 (K_{LDF})	0.05 s^{-1} or higher	0.1 s^{-1}	No
Zeolite 13X (D_{eff}/r_c^2)	8.65E-16 ±1.16E-4 m^2/s	1.09E-15 m^2/s	Yes

Source: Author

4.3.1 Problems with the adsorption method.

After the initial experiments and simulations a few problems concerning the adsorption method arisen, which prompted the change to the desorption method as the standard experimental setup and model. The most evident disadvantage is that the adsorption model is more complex than it's counterpart, more equations and more parameters to determine. However, some experimental constraints are present that makes it difficult to do a reliable measurement.

Following the unexpected results from Zeolite 13X concerning the same value for the diffusional constant at very distant isotherm points, some of the simulated peaks fail to match the experimental data. Figure 4.29 shows one example, this kind of behavior is especially present when the two peaks are done in two different days or in two different experimental batchs. Another somewhat persistent problem is some peaks optimizing at very different values of diffusional constants in comparison with the average results, Figure 4.30.

Figure 4.29 – Peak that resulted in a failed optimization

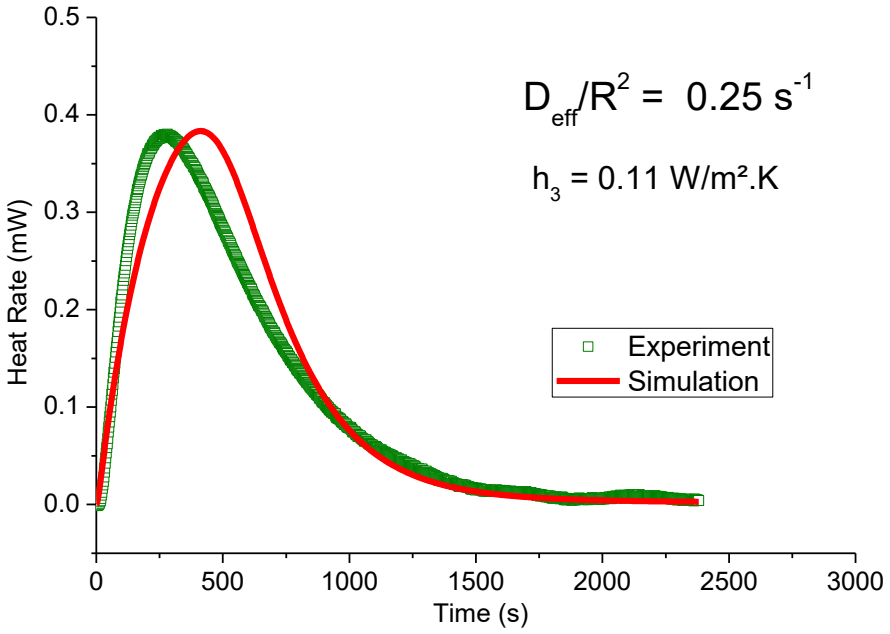

Source: Author

Figure 4.30 – Outlier optimized value

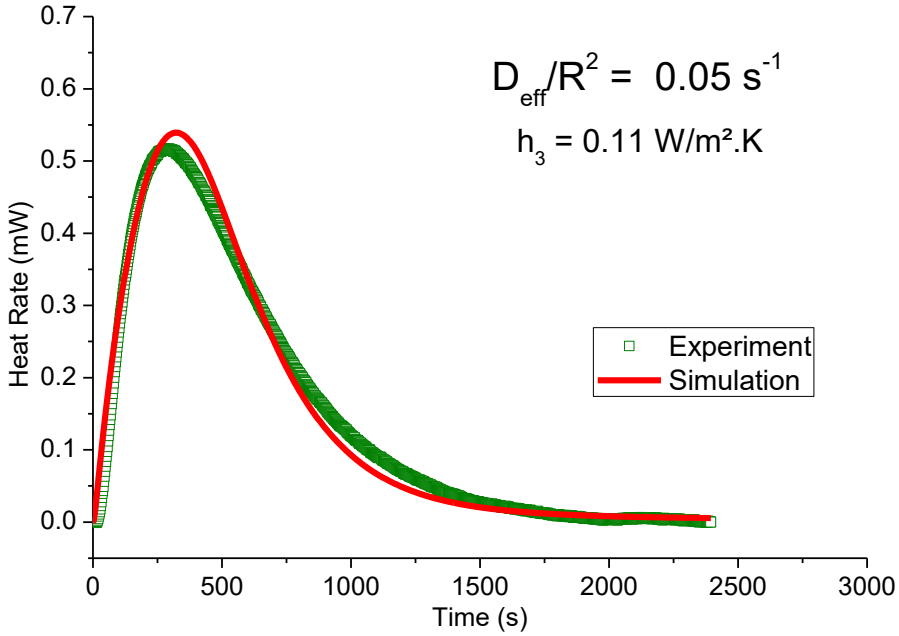

Source: Author

Both of these situations share a common characteristic, the best-fitted value for the kinetic parameter is higher than the average values by two or more orders of magnitude. Explanations based on the effects of secondary mass transfer resistances are discarded, because it is not possible for the overall mass transfer resistance to become lower when more resistances are added, resulting in a faster diffusion.

Possible explanation for this behavior are variations in the heat transfer coefficients, but since the preliminary results were done without the considerations of possible influence of pressure and valve restriction. The analysis for these thermal effects are naturally more complex for the discussed method, due to the possibility of heat effects in the dosing vessel itself.

Thus, for the reasons of a simpler model and for a more controllable experiment, the adsorption method was discarded in favor of the desorption method. An initial test for the reproducibility of the method was done using crystals of Zeolite NaZSM-5 – CO_2 system; the experiments were carried in three different days. Figure 4.31 and Table 4.5 show the Sips isotherm fitting and parameter values, respectively, and Figure 4.32 shows the differential enthalpy curve. Figure 4.33 show the crystal dimensions of the used sample

Table 4.6 – Isotherm parameters adjusted for CO_2 – Zeolite NaZSM-5

Sips Isotherm Parameters	
qm (mmol/g)	2.70
b (Pa^{-1})	7.5E-4
n	0.66

Source: Author

Figure 4.31 – Sips Isotherm Fitting for CO_2 –Zeolite NaZSM-5 system.

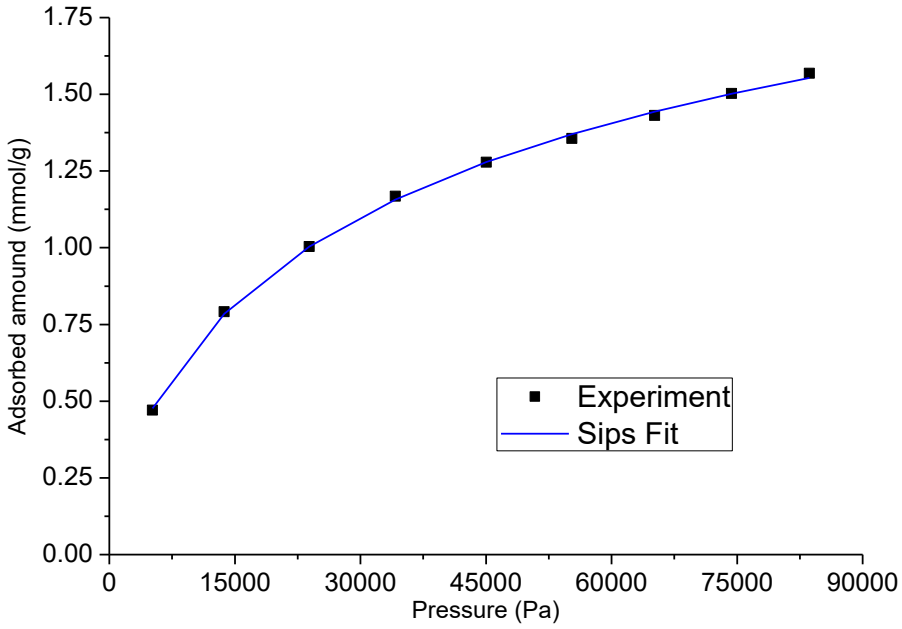

Source: Author

Figure 4.32 – Differential Enthalpy Curve for CO_2 – Zeolite NaZSM-5 system.

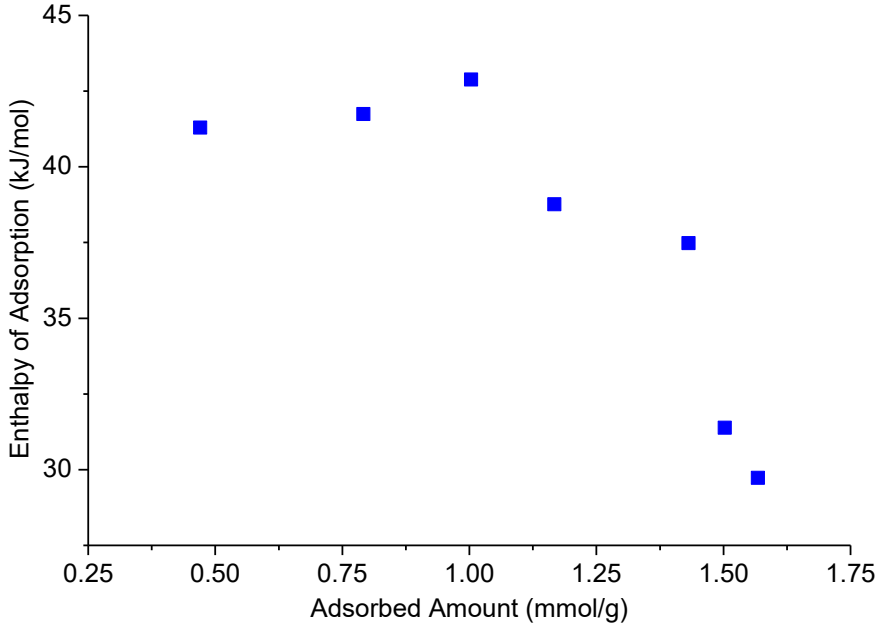

Source: Author

Figure 4.33 – Zeolite NaZSM-5 crystals.

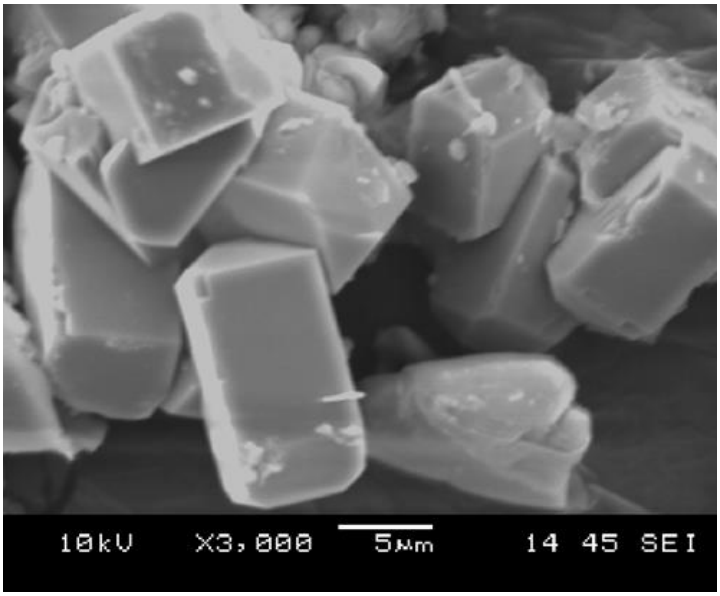

Source: Author

Figures 4.34, 4.35 and 4.36 exhibit the results of the optimizations, the fittings were of high quality and the adjusted diffusional time constants were in the same order of magnitude. The pressure range of the three peaks were in close proximity in terms of the equilibrium isotherm, so no thermodynamic correction is needed, no anomalous behavior took place.

Figure 4.34 – Result of the fitting of the model to experimental results. CO_2 – Zeolite NaZSM-5.Cell Initial pressure: 94556 Pa. Equilibrium Pressure: 90512 Pa. Date: 04/10/2019

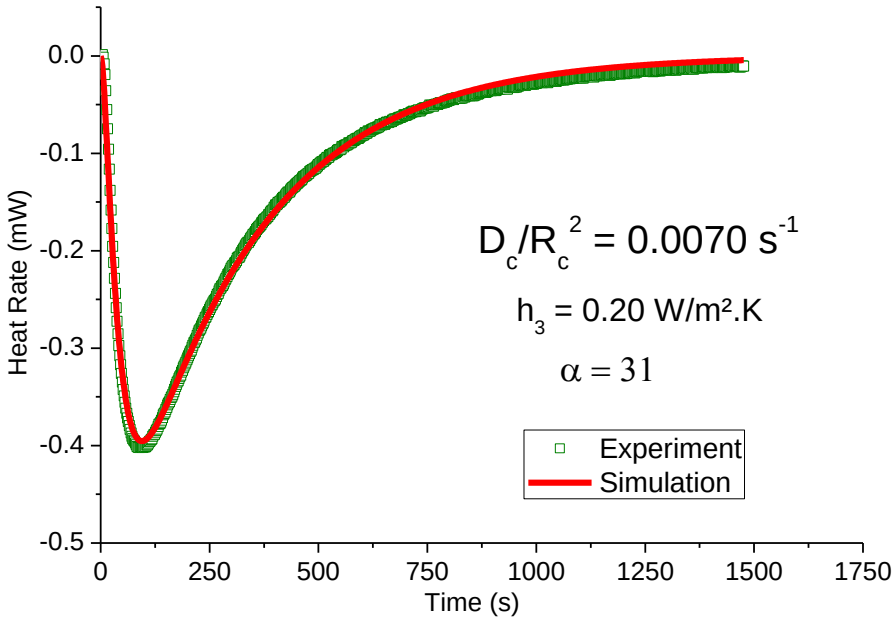

Source: Author

Figure 4.35 – Result of the fitting of the model to experimental results. CO_2 – Zeolite NaZSM-5.Cell Initial pressure: 86506 Pa. Equilibrium Pressure: 81494 Pa. Date: 03/10/2019

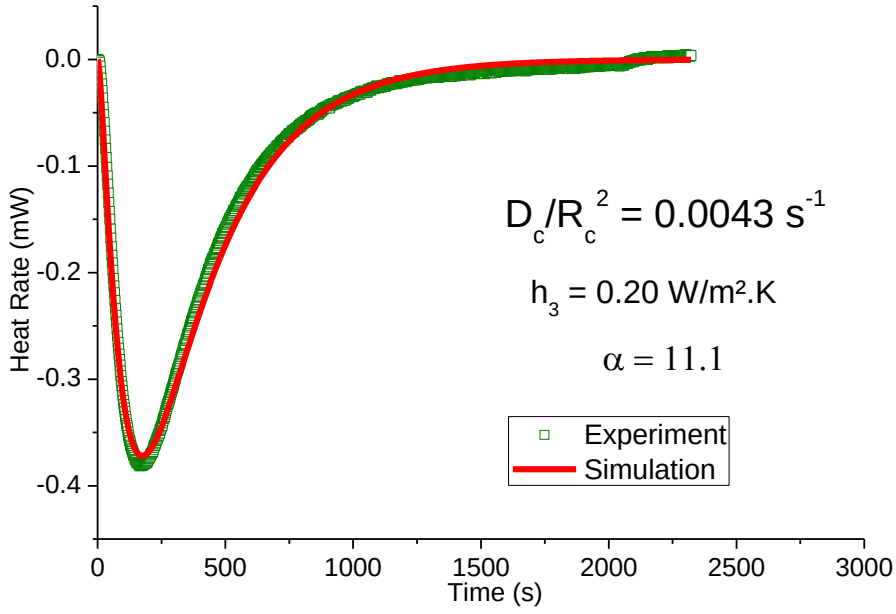

Source: Author

Figure 4.36 – Result of the fitting of the model to experimental results. CO_2 – Zeolite NaZSM-5.Cell Initial pressure: 81818 Pa. Equilibrium Pressure: 76593 Pa. Date: 02/10/2019

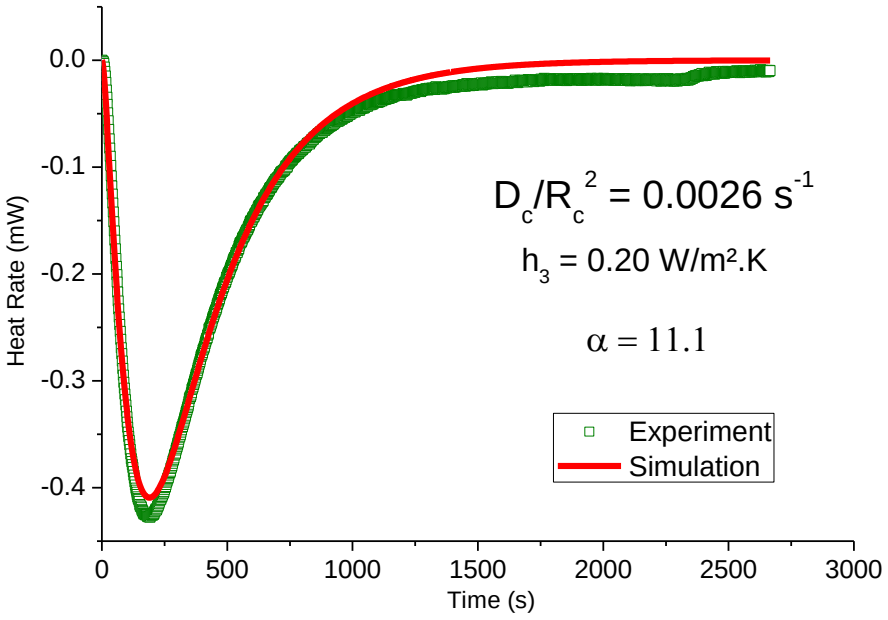

Source: Author

Figures 4.37 and 4.38 show the short time sensitivity of the model to the kinetic constant, two peaks were used because they worked within different valve restrictions, so it is expected different sensibilities, considering the theoretical analysis.

Figure 4.37 – Short time sensitivity of the model at different D_c/r_c^2. CO_2 – Zeolite NaZSM-5 system. Cell Initial pressure: 94556 Pa. Equilibrium Pressure: 90512 Pa. Date: 04/10/2019

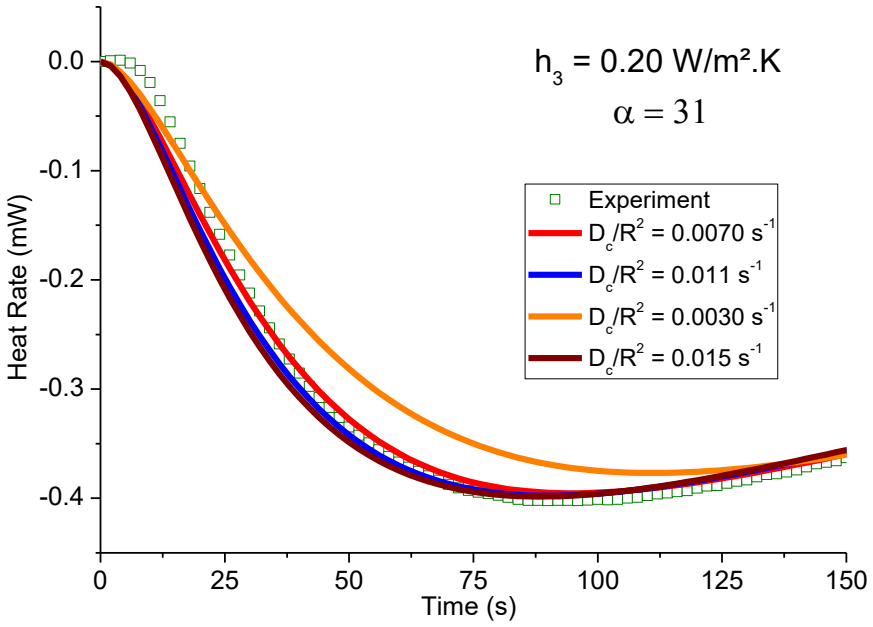

Source: Author

Figure 4.38 – Short time sensitivity of the model at different D_c/r_c^2. CO_2 – Zeolite NaZSM-5 system. Cell Initial pressure: 86506 Pa. Equilibrium Pressure: 81494 Pa. Date: 03/10/2019

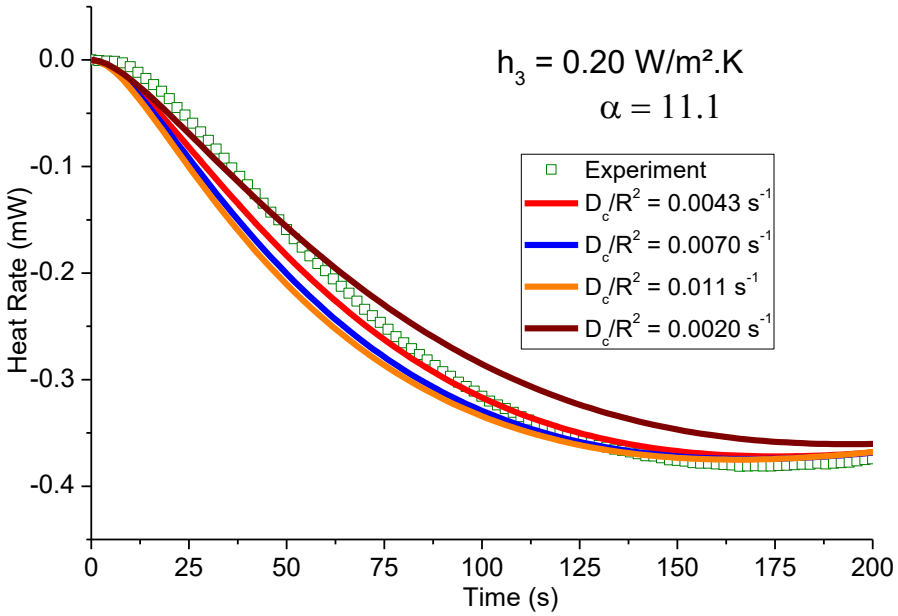

Source: Author

As the graphs show, the peaks have, indeed, different sensibilities and as the theory predicts, the lower sensibility is in the experiment that has the strongest valve restriction. From Figure 4.37, the actual calculated result is anywhere from $\frac{D_c}{r_c^2} = 0.003\ s^{-1}$ and beyond, but for Figure 4.38 the result starts from $\frac{D_c}{r_c^2} = 0.007\ s^{-1}$ and beyond, being the more accurate result. This conclusion is further supported by analysis of the deviations from experimental data, Figure 4.39.

The studied system lacks proper reference measurements in literature, due to the fast diffusion of CO_2 in this Zeolite, which makes it difficult to measure it macroscopically. A molecular simulation paper from Newsome and Coppens (2015) estimates the microscopic self-diffusivity for the present sorbent-sorbate combination, however, since this measurement is at a microscopic level, direct comparisons are not possible, as imperfections in the crystals in larger sizes lead to lower diffusivities, but as a rough estimate, the results were compared at Table 4.6.

Figure 4.39 – Short time sensitivity of the model at different D_c/r_c^2. CO_2 – Zeolite NaZSM-5 system. Average deviation from experimental data

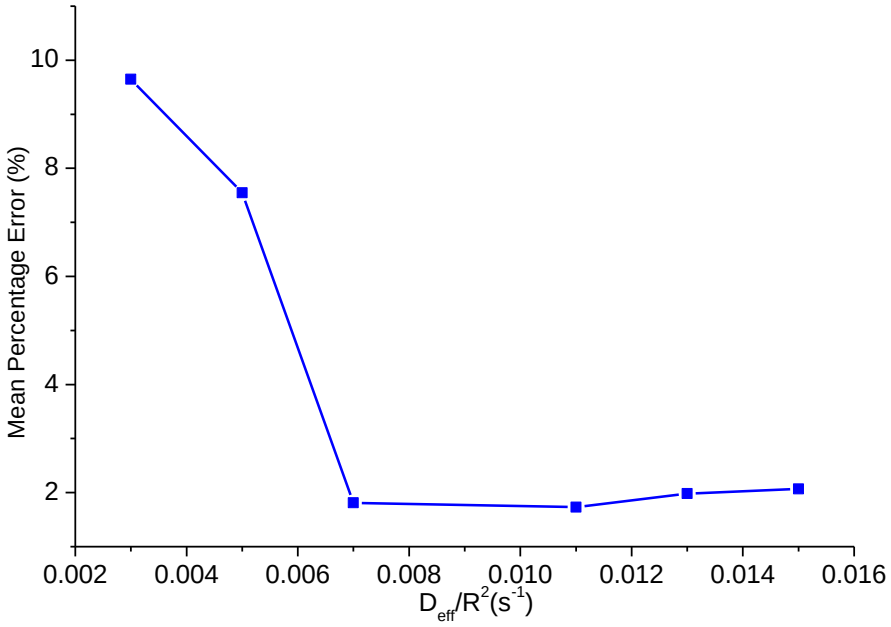

Source: Author

Table 4.7 – Summary of the preliminary desorption results

Calculated kinetic parameters				
Adsorbent	(D_c/r_c^2)	D_c	Literature (self-diffusivity)	Within measurement range?
Zeolite NaZSM-5	0.007 s^{-1} or higher	7.0E-13 m²/s or Higher	2.5E-11 m²/s	No

Source: Author

5 CONCLUSIONS

The semi-theoretical analysis of the model already confirms that a microcalorimetric experiment is sensible to changes in the diffusion coefficients of species, therefore capable of estimating it, if proper experimental conditions are met. The results were consistent with literature, elucidating three relevant resistances on the process: Valve restriction, diffusion and convective heat transfer. It is also concluded that a careful estimation of the heat transfer coefficient is necessary, as it affects the response curve at a very wide range of values. Such estimation is possible on both blank experiments and regular ones, provided that in the latter there is a confirmed presence of a fast-diffusing species, again, a result consistent with

literature. The recommended experimental condition for the measurement of diffusivity, as seen through the model, is an experiment with the lowest valve restriction possible.

Preliminary results confirm the parametric analysis, both in therms of the impact of the valve and the impact of convection on the response curve. Successful fittings of the model into the experimental results demonstrate that it is capable of representing the real ongoing phenomena inside the equipment. However, as the results of NoritRB4 and Zeolite NaZSM-5show, the model has a sensitivity limitation to molecules with fast mass transfer, such as carbon dioxide. Zeolite 13X diffusional time constants were within the range of measurement and the values are reasonably close to those reported in published papers. However the results were not entirely reliable, as it exhibited a few fitting failures for some peaks and some outlier calculated values.

The primary way of estimating the kinetic parameters was changed from an adsorption experiment to a desorption one. The reasons were both on the side of a simpler model and due to a much more controllable experiment, the initial desorption results showed high quality fittings and a better statistical behavior of the measured diffusivities.

The use of blank experiments to calculate heat transfer parameters proved effective, although the results point to a different value for heat parameters for each adsorbent, which could be explained by fluid stagnation effects caused by different particle sizes. Therefore, for every calorimetric experiment done for a sample, a blank experiment should be also performed to determine the heat transfer coefficient for that sample.

The final conclusion of this work is a general guideline for the appropriate use of microcalorimetry for the evaluation of mass transfer parameters. First, valve restrictions on the experiments should be as low as possible. Second, the heat transfer parameters should be carefully evaluated with precision, as it has a very significant effect on the response curve; each adsorbent should have a specific convective heat transfer parameter in the system. Third, after all parameters are at hand, the adsorptive model should be fitted to the experimental results, optimizing the mass transfer parameter. Fourth, after the parameter is optimized, a sensitivity analysis is necessary to ensure that the calculated value is at the bounds of measurement, if the mass transfer resistance is too low compared to other resistances, the model is only capable of calculating a lower limit for the diffusivities. Lastly, as a recommendation, the use of desorption experiments are generally more suited for this task, due to simpler model and better experimental control.

Future works may include testing with slower diffusing species, such as hydrocarbons, which have also a larger source of results published in literature for validations. Comparison

with already existing methods is also pertinent, as to evaluate not only the effectiveness of the calorimetric method, but also the opportunity costs in relation to the widely used experimental techniques and models.

REFERENCES

BHATIA, S. K.; JEPPS, O.; NICHOLSON, D. Tractable molecular theory of transport of Lennard-Jones fluids in nanopores. **The Journal of Chemical Physics**. v. 120. n. 9. p. 4472–4485.

BRANDANI, S. Analysis of the Piezometric Method for the Study of Diffusion in Microporous Solids: Isothermal Case. **Adsorption**. v. 4, p. 17, 1998.

BRUANUER, S.; EMMETT, P. H.; TELLER, E. Adsorption of gases in multimolecular layers, **J. Am. Chem. Soc**. v. 60, p. 309–316, 1938.

DARKEN L. S. Diffusion, mobility and their interrelation through free energy in binary metallic systems. **Trans. AIME**. v. 175, p. 184-201, 1948.

DO, D. D. **Adsorption Analysis: Equilibria and Kinetics, Chemical Engineer Series.** 1. ed. London: Imperial College Press, 1998. 892 p.

DRAKE, J. M.; KLAFTER, J. Dynamics of Confined Molecular Systems. **Physics Today**. v. 43, n. 5, p. 46–55, 1990.

EIC, M.; RUTHVEN, D. M. A new experimental technique for measurement of intracrystalline diffusivity. **Zeolites**. v.8, n. 1, p. 40–45, 1988.

EINSTEIN, A. Zur Theorie der Brownschen Bewegung. **Ann. Phys**. v. 19, n. 371, 1906.

ERTL, G. Reactions at Surfaces: From Atoms to Complexity (Nobel Lecture). **Angewandte Chemie International Edition**. v. 47, n. 19, p. 3524–3535, 2008.

FOO, K. Y.; HAMEED, B. H. Insights into the modeling of adsorption isotherm systems. **Chemical Engineering Journal**. v. 156, n. 1, p. 2–10, 2010.

FREUNDLICH, H. M. F. Over the adsorption in solution, **J. Phys. Chem**. v. 57, p. 385–471, 1906.

GLUECKAUF, E. Theory of chromatography. Part 10 – Formulae for diffusion into spheres and their application to chromatography. **Trans. Faraday Soc**. v. 51, p. 1540-1551, 1955.

GRENIER, P.; MEUNIER, F.; GRAY, P. G.; KÄRGER, J.; XU, Z.; RUTHVEN, D. M. Diffusion of methanol in NaX crystals: Comparison of i.r., ZLC, and PFG-n.m.r. measurements. **Zeolites**. v. 14, n. 4, p. 242–249, 1994.

GRENIER, P.; BOURDIN, V.; SUN, L. M.; MEUNIER, F. Single-step thermal method to measure intracrystalline mass diffusion in adsorbents. **AIChE Journal**. v. 41 n. 9, p. 2047–2057, 1995.

HAYNES, H. W. The Experimental Evaluation of Catalyst Effective Diffusivity. **Catalysis Reviews**. v .30, n. 4, p. 563–627, 1988.

KÄRGER, J.; RUTHVEN, D. M., THEODOROU, D. N. **Diffusion in nanoporous materials**. 1. ed. Germany: Wiley-VCH, 2011. 902 p.

KELLER, J.; STAUDT, R. **Gas Adsorption Equilibria**. 1. ed. Berlin: Springer, 2004. 422 p.

LAERI, F.; SCHEUTH, F.; SIMON, U.; WARK, M. **Host-Guest Systems Based on Nanoporous Crystals**. 1. ed. Weinheim: Wiley-VCHVerlag GmbH, 2003. 662 p.

LANGMUIR, I. The constitution and fundamental properties of solids and liquids, **J. Am. Chem. Soc**. v. 38, n. 11, p. 2221–2295, 1916.

LIMOUSIN, G.; GAUDET, J. P.; CHARLET, L.; SZENKNECT, S.; BARTHÈS, V.; KRIMISSA, M. Sorption isotherms: A review on physical bases, modeling and measurement. **Applied Geochemistry**. v. 22, n. 2, p. 249–275. 2007.

LLEWELLYN, P. L.; G. MAURIN. Gas adsorption microcalorimetry and modelling to characterise zeolites and related materials, **Comptes Rendus Chim**. v. 8 n. 3–4, p. 283–302, 2005.

MAIA, D. A. S.; DE OLIVEIRA, A. J. C.; NAZZARRO, M. S.; SAPAG K. M.; LÓPEZ R. H.; LUCENA, S. M. P.; DE AZEVEDO, D. C. S. CO_2 gas-adsorption calorimetry applied to the study of chemically activated carbons. **Chem. Eng. Res. Des**. v. 136, p. 753–760, 2018.

MAIA, D. A. S. **Estudios Sistemáticos, combinando Métodos Experimentales Calorimétricos y de Simulación, para el Desarrollo de Carbones Activados para la Adsorción de CO_2**. 2014. Thesis (PhD in Chemical Engineering) – Universidad Nacional de San Luis, San Luis, 2014.

THOMMES, M.; KANEKO, K.; NEIMARK, A. V.; OLIVIER, J. P.; REINOSO, F. R.; ROUQUEROL, J.; SING, K. S. W. Physisorption of gases, with special reference to the evaluation of surface area and pore size distribution. **IUPAC Technical Report**, 2015.

NEWSOME, D.; COPPENS, M. O. Molecular dynamics as a tool to study heterogeneity in zeolites – Effect of Na+ cations on diffusion of CO_2 and N_2 in Na-ZSM-5. **Chemical Engineering Science**. v. 121, p. 300–312, 2015.

NICHOLSON, D.; PETROPOULOS, J. H. Calculation of the “surface flow” of a dilute gas in model pores from first principles. **Journal of Colloid and Interface Science**. v. 106 n. 2, p. 538–546, 1985.

RAGHAVAN, N. S.; RUTHVEN, D. M. Simulation of chromatographic response in columns packed with bidisperse structured particles. **Chemical Engineering Science**. v. 40 n. 5, p. 699–706, 1985.

ROUQUEROL, F.; ROUQUEROL, J.; SING, K. S. W.; LLEWELLYN P. L.; MAURIN, G. **Adsorption by Powder & Porous Solids – Principles Methodology and Applications**. 2. ed. London: Academic press, 2014. 646 p.

ROUQUEROL, F.; ROUQUEROL, J.; EVERETT, D. H. Gas-solid interactions. General derivation of reaction enthalpies from the data of isothermal microcalorimetry. **Thermochim. Acta**. v. 41, p. 311–322, 1980.

ROUQUEROL, F.; ROUQUEROL, J.; SING, K. S. W. 1999. **Adsorption by Powders and Porous Solids**. 1. ed. San Diego: Academic Press, 1999. 467 p.

RUTHVEN, D. M.; EIC, M. Intracrystalline diffusion in zeolites. Perspectives in Molecular Sieve Science, **ACS Symp. Ser. Washington**. v. 368, p. 362-375, 1988.

RUTHVEN, D. M.; KUMAR, R. A chromatographic study of the diffusion of N2, CH4 and binary CH_4-N_2 mixtures in 4A molecular sieve. **The Canadian Journal of Chemical Engineering**. v. 57, n. 3, p. 342–348, 1979.

RUTHVEN, D. M.; LEE, L. K. Kinetics of nonisothermal sorption: Systems with bed diffusion control. **AIChE Journal**. v. 27 n. 4, p. 654–663, 1981.

RUTHVEN, D. M.; FAROOQ, S.; KNAEBEL, K. S. **Pressure Swing Adsorption**. 1. ed. New York: Wiley-VCH, 1994. 376 p.

RUTHVEN, D. M. **Principles of Adsorption and Adsorption processes**. 1. ed. New York: John Wiley & Son, 1984. 453 p.

SCHUMACHER, R.; EHRHARDT, K.; KARGE, H. G. Determination of Diffusion Coefficients from Sorption Kinetic Measurements Considering the Influence of Nonideal Gas Expansion. **Langmuir**. v. 15, n. 11, p. 3965–3971, 1999.

SILVA, J. A. C.; SCHUMANN, K.; RODRIGUES, A. E. Sorption and kinetics of CO_2 and CH_4 in binderless beads of 13X zeolite. **Microporous and Mesoporous Materials**. v. 158, p. 219–228, 2012.

SING, K. S. W.; EVERETT, D. H.; HAUL, R. A. W.; MOSCOU, L.; PIEROTTI, R. A.; ROUQUÉROL, J.; SIEMIENIEWSKA, T. Reporting physisorption data for gas/soils systems with special reference to the determination of surface area and porosity. Commission on Colloid and Surface Chemistry Including Catalysis, Physical Chemistry Division, **International Union of Pure and Applied Chemistry (IUPAC)**. Pure Applied Chemistry, v. 57, n. 4, p. 603-619, 1985.

SIPS, R. Combined form of Langmuir and Freundlich equations, **J. Chem. Phys**. v. 16, p. 490–495, 1948.

SIQUEIRA, R. M; VILARRASA-GARCIA, E.; TORRES, A. E. B; DE AZEVEDO, D. C. S.; BASTOS-NETO, M. Simple Procedure to Estimate Mass Transfer Coefficients from Uptake Curves on Activated Carbons. **Chem. Eng. Technol**. v. 41 n. 8, p. 1622–1630, 2018.

TOTH, J. State equations of the solid gas interface layer. **Acta Chem. Acad. Hung**. v. 69, p. 311–317, 1971.